2. Subjects and methods

2.1. Study population

The Atomic Bomb Casualty Commission, subsequently the RERF, established the AHS cohort in 1958. This cohort study enrolled a total of 23,000 atomic bomb survivors in Hiroshima and Nagasaki who biennially received health examinations in outpatient clinics [11]. Hepatitis screening (HBsAg, anti-HBc antibody (Ab), anti-HBs Ab, and anti-HCV Ab tests, as well as HCV RNA test if the anti-HCV Ab was positive) was conducted among 6,121 AHS participants in 1993–1995 [12]. Anti-HCV Ab negative subjects were categorized as the HCV-uninfected group in this study, whereas a "persistence" group was identified by anti-HCV Ab positive with detected HCV RNA, and a "spontaneous clearance" group was identified by anti-HCV Ab positive and undetectable HCV RNA. Subjects who were hepatitis B virus surface antigen positive were excluded from this study. From the 6,121 AHS subjects, lymphocyte subsets in the peripheral blood were then examined in 162 HCV persistence, 145 virus clearance, and 3,511 uninfected subjects in 2000–2002. Most subjects (n = 120, 74%) in the persistence group (n = 162, including those with cancer history) were confirmed by a second RNA test at least 2 years after the first RNA test performed in 1993–1995. Although the remaining 42 subjects in the group did not undergo the second RNA test, these subjects were confirmed to have developed type C chronic liver disease based on medical chart review (*e.g.*, treatment history, abdominal sonographic observation, changes in platelet counts, zinc sulfate turbidity, aspartate aminotransferase (AST), and alanine aminotransferase (ALT) between 1993–1995 and 2000–2002) by a hepatologist (one of the authors, WO). Subsequent treatment data of hepatitis C from attending physicians were also taken into account. No subjects in the persistence group underwent interferon (IFN) therapy in 2000–2002.

This study was approved by the RERF Human Investigation Committee, and all subjects gave written informed consent before each examination.

2.2. Assays in hepatitis screening and clinical examinations

In 1993–1995, anti-HCV Ab and hepatitis B virus surface antigen were examined using a second-generation passive hemagglutination kit and a reverse passive hemagglutination kit (Dynabott, Tokyo), as described previously [12]. Subjects were diagnosed as having Ab when agglutination was reported in a serum diluted 2^5. Qualitative and quantitative detection of HCV RNA was carried out using the Amplicor HCV ver. 2.0 and the Amplicor HCV monitor test ver. 1.0 and/or ver. 2.0 (Roche Diagnostics Systems, Tokyo, Japan).

Platelet count decreases with progression of liver fibrosis, and this marker has widely been used as a reliable diagnostic tool for liver fibrosis/cirrhosis in patients with chronic HCV infection [13–16]. Postulated mechanisms for such platelet reduction include decreased secretion of the hematopoietic growth factor thrombopoietin from the liver and increased destruction of platelets by antiplatelet antibodies [17,18]. Platelet count was routinely measured in the AHS health examination, and an automatic blood cell counter (Coulter MAXM, Beckman Coulter, Inc, Tokyo, Japan) was used in 2000–2002. AST, ALT, γ-glutamyltransferase (γ-GTP), and total cholesterol were also routinely measured, and an autoanalyzer (Hitachi 7180, Hitachi, Ltd., Tokyo, Japan) was used in 2000–2002.

2.3. Information on lifestyle/environmental factors and clinical data

Information on alcohol drinking and smoking was obtained from questionnaires at the time of the AHS health examination in 1993–1995 and 2000–2002, respectively. Body mass index (BMI) was measured at the AHS health examination in 2000–2002. Radiation dose was estimated by the DS02 dosimetry system [19], based on the weighted skin dose computed as the γ dose plus 10 times the neutron dose. No subjects were diagnosed with human immunodeficiency virus infection. No subjects underwent organ transplantation or immunosuppressive therapy. Clinical information was obtained at the AHS examination in 2000–2002 as well as medical chart review and classified according to the International Classification of Diseases code.

2.4. Lymphocyte subset analysis

Circulating T_H1 and T_H2 cells can be straightforwardly enumerated by flow cytometry, using cell surface markers for chemokine receptor, CXCR3, and prostaglandin D receptor, CRTH2, respectively [20,21]. CD8 T cells expressing CXCR3, known as T_C1, are also involved in viral control during HCV infection [22]. We thus focused on T_H1, T_H2, T_C1, and T_C2 cell subsets, as well as total CD4 T and CD8 T, NK, and B-cell subsets in relation to HCV infection status.

Analytical flow cytometry was conducted in a FACScan machine (BD Biosciences, San Jose, CA) as described previously [23]. Monoclonal antibodies as specific cell surface markers were purchased from BD Pharmingen (San Diego, CA), unless otherwise noted. CD4 or CD8 T cells were enumerated as PerCP-labeled CD3 positive and PE–CD4 or FITC–CD8 positive cells; CD16 or CD20 cells were enumerated as PerCP–CD3 negative and FITC–CD16 (Beckman Coulter, Brea, CA) or PE–CD20 positive cells. We used CXCR3 as a marker for T_H1 and T_C1 cells [20,22] and CRTH2 for T_H2 and T_C2 cells [21]. Namely, T_H1 and T_H2 cells were identified with PerCP–CD4, FITC–CXCR3 (R&D Systems, Minneapolis, MN), and biotinylated CRTH2 (kindly provided by Dr K. Nagata, BML, Kawagoe, Japan) plus PE-streptavidin; T_C1 and T_C2 cells were identified with PerCP–CD8, FITC–CXCR3, and biotinylated CRTH2 plus PE–streptavidin. In every measurement, approximately 20,000 cells were analyzed.

2.5. Statistical analysis

Two-sample Wilcoxon or Pearson χ^2 tests were performed to compare distributions of age, gender, city, radiation dose (Gy), smoking (packs/day), alcohol drinking (converted to grams of ethanol/day), BMI (kg/m^2), AST (IU/L), ALT (IU/L), γ-GTP (U/L), total cholesterol (mg/dL), and platelet count ($\times 10^4/\mu$L) among all combinations of the 3 groups.

Because aging and past radiation exposure likely influenced various immunologic markers [23], these events were also evaluated in this study. In each study group, the associations of lymphocyte subsets with age (at the time of examination), gender, radiation dose, and city were evaluated based on the multiple regression model [24]:

$$\log(\textit{subset percentages or ratios}) = \alpha + \beta_1 \times \textit{age} + \beta_2 \times \text{gender} + \beta_3 \times \text{dose} + \beta_4 \times \text{city} + \beta_5 \times \text{alcohol} + \beta_6 \times \text{smoking} + \beta_7 \times \text{BMI} + \beta_8 \times \text{autoimmune disease} + \beta_9 \times \text{allergic disease} + \beta_{10} + \textit{cancer} + \beta_{11} \times \text{other noncancer diseases},$$

where log is the logarithm at base 10, gender = 0 for male and 1 for female, and city = 1 for Hiroshima and 2 for Nagasaki. Smoking, alcohol drinking, BMI, autoimmune disease (1 if diagnosed, otherwise 0), allergic disease (1 or 0), cancer (1 or 0), and other noncancer diseases (*i.e.*, hypergammaglobulinemia and sarcoidosis, 1 or 0) were also used as additional explanatory variables.

We compared lymphocyte subset percentages or ratios among all combinations of the 3 groups in normal regression analysis with adjustment for age, gender, radiation dose, city, alcohol, smoking, BMI, autoimmune diseases, allergic diseases, and other noncancer diseases: In the regression analysis, an explanatory variable regarding a group (1 group = 0, another group = 1) was used.

Regression analysis was also performed to investigate whether any association existed between subset percentages or ratios and

Table 1
Characteristics of the study subjects

	Persistence (anti-HCV+/ HCV RNA+) (n = 162)	Clearance (anti-HCV+/ HCV RNA-) (n = 145)	Uninfected (anti-HCV-) (n = 3,511)	Persistence vs clearance (p)[a]	Persistence vs uninfected (p)[a]	Clearance vs uninfected (p)[a]
Age[b]	71.7 (60.8–83.0)	72.3 (64.8–88.0)	72.2 (58.4–87.2)	0.041	0.79	0.029
Gender[c]						
Male	57 (35.2)	48 (33.1)	1078 (30.7)	0.70	0.23	0.54
Female	105 (64.8)	97 (66.9)	2433 (69.3)			
City[c]						
Hiroshima	112 (69.1)	96 (66.2)	2034 (57.9)	0.58	0.005	0.048
Nagasaki	50 (30.9)	49 (33.8)	1477 (42.1)			
Radiation dose (Gy)[b]	0.147 (0–2.658)	0.071 (0–1.890)	0.096 (0–2.032)	0.26	0.47	0.39
Smoking (packs/day)[b]	0 (0–1.0)	0 (0–1.0)	0 (0–1.0)	0.80	0.087	0.18
Alcohol drinking (grams/day)[b]	0 (0–85.0)[d]	0 (0–103.0)[d]	0 (0–69.8)[d]	0.35	0.57	0.062
BMI (kg/m^2)[b]	22.4 (16.7–28.5)	22.6 (17.3–29.6)	22.7 (17.6–28.7)	0.46	0.084	0.58
AST (IU/L)[b]	21 (15–51)	21 (14–35)	22 (15–43)	0.15	0.85	0.081
ALT (IU/L)[b]	17 (9–46)	18 (9–42)	17 (9–44)	0.87	0.99	0.84
γ-GTP (U/L)[b]	28.5 (12.5–131.5)	25 (12–127)	24 (11–111)	0.10	<0.001	0.29
Total cholesterol (mg/dL)[b]	168.5 (117–234)	206 (142–264)	208 (154–266)	<0.001	<0.001	0.41
Platelet count (×10^4/μL)[b]	17.3 (7.2–28.2)	22.0 (14.3–30.8)	22.9 (14.5–33.7)	<0.001	<0.001	0.031

[a]Two-sample Wilcoxon rank-sum test or Pearson's χ^2 test for gender and city.
[b]Median (5–95% percentiles).
[c]Number (%).
[d]The percentages of never-drinkers were 59.3, 53.8, and 60.6 in the 3 groups, respectively.

time-course changes in platelet counts through the period from 2000 through 2006. Changes in platelet counts were calculated by the following method:

(platelet counts at the last examination

– platelet counts at the first examination)/follow-up years

In a regression analysis, a forward stepwise procedure was used for 8 immunologic variables, %CD4, T_H1, T_H2, CD8, T_C1, T_C2, CD16, and CD20. Four variables (%T_H1, T_C1, CD16, and CD20) were consequently selected (significance level to select, $p < 0.2$) to construct a statistical model. All analyses were conducted using Stata software (Stata/SE 9.2 for Windows, StataCorp LP, College Station, TX).

3. Results

3.1. Basic characteristics of study subjects

Table 1 compares characteristics of study subjects in the HCV persistence, clearance, and uninfected groups. The persistence group exhibited increased levels of blood γ-GTP and decreased levels of total cholesterol and platelet counts compared with the other 2 groups, indicating enhanced liver injury by persistent HCV infection. The proportion of Hiroshima subjects in the persistence or clearance group was higher than that in the uninfected group. This is in accordance with the previous study that indicated a higher anti-HCV Ab prevalence in Hiroshima atomic bomb survivors than in Nagasaki survivors [12]. There were no significant differences in radiation dose by HCV infection status.

This study primarily aimed to evaluate immunologic alterations associated with HCV infection that might be modulated by age, gender, or past radiation exposure. Therefore, the effects of those factors on lymphocyte subsets were first analyzed and are summarized in the supplemental tables. In the uninfected group, we observed the following: (i) age- and dose-dependent decreases in total CD4 T cell percentages, (ii) higher total CD4 T-cell percentages in females than in males, (iii) no significant effects of age, gender, or radiation dose on total CD8 T-cell percentages, (iv) increased CD16 (NK) cell percentages with increasing age and higher percentages in males than in females, (v) increased T_H1 and T_H2 cell percentages with increasing age and dose, and (vi) both T_H1/T_H2 and T_C1/T_C2 cell ratios negatively or positively associated with age and female gender, respectively, but not with radiation dose (Suppl. Table 1). The

Table 2
Characteristics of the study subjects with no cancer history

	Persistence (anti-HCV+/ HCV RNA+) (n = 102)	Clearance (anti-HCV+/ HCV RNA-) (n = 113)	Uninfected (anti-HCV-) (n = 2,813)	Persistence vs clearance (p)[a]	Persistence vs uninfected (p)[a]	Clearance vs uninfected (p)[a]
Age[b]	71.5 (61.3–82.7)	72.3 (62.4–90.8)	72.0 (58.1–87.3)	0.026	0.64	0.021
Gender[c]						
Male	36 (35.3)	38 (33.6)	832 (29.6)	0.80	0.22	0.36
Female	66 (64.7)	75 (66.4)	1981 (70.4)			
City[c]						
Hiroshima	70 (68.6)	77 (68.1)	1613 (57.3)	0.94	0.023	0.023
Nagasaki	32 (31.4)	36 (31.9)	1200 (42.7)			
Radiation dose (Gy)[b]	0.031 (0–1.862)	0.056 (0–1.890)	0.072 (0–1.878)	0.84	0.68	0.49
Smoking (packs/day)[b]	0 (0–1.0)	0 (0–1.0)	0 (0–1.0)	0.67	0.070	0.18
Alcohol drinking (grams/day)[b]	0 (0–90)[d]	0 (0–105.8)[d]	0 (0–69.8)[d]	0.067	0.76	0.014
BMI (kg/m^2)[b]	22.6 (16.7–28.5)	22.6 (17.3–29.6)	22.9 (17.7–28.8)	0.49	0.097	0.55
AST (IU/L)[b]	22 (15–50)	21 (13–37)	22 (15–42)	0.12	0.34	0.26
ALT (IU/L)[b]	18 (9–39)	17 (9–48)	17 (9–44)	0.57	0.69	0.69
γ-GTP (U/L)[b]	26 (12–100)	27 (12–127)	23 (11–106)	0.99	0.19	0.18
Total cholesterol (mg/dL)[b]	175 (124–243)	211 (136–272)	209 (157–266)	<0.001	<0.001	0.46
Platelet count (×10^4/μL)[b]	19.3 (10.3–32.0)	21.7 (14.2–30.8)	23.0 (14.8–33.7)	<0.001	<0.001	0.006

[a]Two-sample Wilcoxon rank-sum test, or Pearson's χ^2 test for gender and city.
[b]Median (5–95% percentiles).
[c]Number (%).
[d]The percentages of never-drinkers were 64.7, 50.4, and 61.1 in the 3 groups, respectively.

Table 3
Comparisons of peripheral lymphocyte subsets among subjects with no cancer history

	Persistence (n = 102)	Clearance (n = 113)	Uninfected (n = 2,813)	Persistence vs clearance (p)[a]	Persistence vs uninfected (p)[a]	Clearance vs uninfected (p)[a]
CD4 (%)[b]	40.8 (8.9)	42.2 (9.0)	43.0 (8.9)	0.32	0.007	0.46
T_H1 (%)[b]	35.2 (9.6)	27.1 (8.7)	26.0 (8.9)	<0.001	<0.001	0.23
T_H2 (%)[b]	1.55 (0.88)	1.74 (1.03)	1.79 (1.10)	0.54	0.11	0.65
T_H1/T_H2[b]	30.7 (20.6)	20.8 (12.8)	20.8 (23.0)	<0.001	<0.001	0.27
CD8 (%)[b]	23.4 (9.6)	20.9 (7.9)	19.0 (7.8)	0.20	<0.001	0.040
T_C1 (%)[b]	42.3 (14.7)	38.8 (15.2)	39.5 (14.6)	0.25	0.17	0.68
T_C2 (%)[b]	2.78 (3.72)	2.87 (4.03)	3.35 (5.09)	0.34	0.68	0.40
T_C1/T_C2[b]	42.8 (45.8)	50.9 (78.2)	51.1 (91.4)	0.66	0.38	0.51
CD4/CD8[b]	2.08 (1.02)	2.42 (1.35)	2.75 (1.57)	0.15	<0.001	0.054
CD16 (%)[b]	14.0 (9.4)	17.0 (8.8)	17.1 (9.4)	0.035	<0.001	0.82
CD20 (%)[b]	14.5 (7.6)	13.5 (5.3)	13.9 (6.1)	0.95	0.44	0.60

[a]Test of difference of logarithmic values between 2 groups using normal regression analysis with adjustment for age, gender, city, radiation dose, alcohol, smoking, BMI, autoimmune disease, allergic disease, and other noncancer diseases.
[b]Mean (SD).

persistence and clearance groups also demonstrated similar associations, although most associations were not statistically significant, probably because of the smaller numbers of subjects in these groups (Suppl. Tables 2 and 3). In addition to the 3 factors (age, gender, and radiation), other selected factors, such as city, alcohol, smoking, and BMI, also influenced various lymphocyte subsets (data not shown), and they were used as confounding variables in adjustments.

3.2. Comparison of lymphocyte subsets among the HCV persistence, clearance, and uninfected groups

The study subjects having cancer history numbered 60, 32, and 698 in the persistence, clearance, and uninfected groups, respectively. We then analyzed the lymphocyte subset alterations associated with HCV infection among subjects who have no history of cancer, presented in Table 2, to eliminate potential effects of cancer development and/or cancer therapy (Table 3). In addition, basic characteristics were not largely changed by excluding subjects with a history of cancer, but the radiation effects—specifically on T_H1 and T_H2 cells—were no longer seen among subjects with no cancer history (data not shown).

In the persistence group, T_H1 and total CD8 T cell percentages and T_H1/T_H2 ratios were significantly higher than those in the HCV-uninfected group, whereas total CD4 T and CD16 cell percentages were lower. Similar differences were also seen between the persistence and clearance groups. However, except for total CD8 T cell percentages, no significant differences were observed between the clearance and uninfected groups.

3.3. Relationship between lymphocyte subsets and progression of liver fibrosis in the HCV persistence group

Next, we analyzed the relationship between lymphocyte subsets and platelet counts that had been longitudinally examined at the biennial AHS examination during 2000–2006 in the HCV persistence group, excluding subjects with cancer history (Table 4). The average follow-up period was 4.7 years, and the average decrement of platelet counts per year was -0.75 ($\times 10^4/\mu L$). We determined that increased percentages of T_H1 cells were associated with accelerated time-course reduction in platelet counts—accelerated progression of liver fibrosis ($p = 0.027$)—whereas T_C1 and NK cell percentages were inversely associated with progression ($p = 0.027$ and 0.058, respectively).

4. Discussion

We investigated immunologic alterations associated with HCV infection in a longevity study cohort of atomic bomb survivors. First, the effects of age, gender, and radiation on total CD4 T, CD8 T, and NK cells were studied in the uninfected group (Suppl. Table 1) and observed to be in close agreement with our previous studies [9,23]. A new finding related to the uninfected group is that percentages of both T_H1 and T_H2 cells increased with increasing radiation dose and age. That result is consistent with our previous

Table 4
Regresson analysis of decrements (per year) in platelet counts among HCV persistence subjects with no cancer history (N = 96)

Explanatory variables	Unadjusted coefficient	p	Adjusted[a] coefficient	p	Adjusted[b] coefficient	p
Age (+10 years)	−0.26	0.33	–	–	–	–
Gender (female vs male)	0.43	0.21	–	–	–	–
Radiation dose (Gy)	0.28	0.26	–	–	–	–
City (Nagasaki vs Hiroshima)	0.00	0.99	–	–	–	–
Log CD4	−0.25	0.86	1.11	0.50	–	–
Log T_H1	−1.90	0.13	−2.38	0.086	−3.19	0.027
Log T_H2	−0.53	0.41	−0.34	0.65	–	–
Log T_H1/T_H2	0.03	0.97	−0.31	0.67	–	–
Log CD8	−1.72	0.060	−2.63	0.011	–	–
Log T_C1	1.66	0.068	2.05	0.041	2.36	0.027
Log T_C2	−0.30	0.37	0.23	0.57	–	–
Log T_C1/T_C2	0.51	0.12	0.10	0.81	–	–
Log CD4/CD8	1.04	0.16	2.03	0.015	–	–
Log CD16	0.73	0.21	1.13	0.062	1.18	0.058
Log CD20	1.10	0.11	1.04	0.15	1.03	0.17

[a]Regression model: decrements in platelet counts = $\alpha + \beta_1 \times log$(lymphocyte subset) + $\beta_2 \times$ age + $\beta_3 \times$ gender + $\beta_4 \times$ dose + $\beta_5 \times$ city + $\beta_6 \times$ alcohol + $\beta_7 \times$ smoking + $\beta_8 \times$ BMI + $\beta_9 \times$ autoimmune disease + $\beta_{10} \times$ allergic disease + $\beta_{11} \times$ other noncancer diseases.
[b]Forward stepwise procedure ($p < 0.2$) was used for 8 lymphocyte variables (CD4, T_H1, T_H2, CD8, T_C1, T_C2, CD16, and CD20). Four selected variables (T_H1, T_C1, CD16, and CD20) were used in the regression analysis with the 10 explanatory variables in footnote a.

findings in an expanded cohort of atomic bomb survivors, which demonstrated age- and radiation dose-dependent elevations of cytokine levels for both T_H1-related cytokines (IFN-γ and tumor necrosis factor-α) and a T_H2-related cytokine (interleukin [IL]-6) [25].

Second, we observed that persistent HCV infection was associated with increases in T_H1/T_H2 cell ratios and CD8 T cell percentages and a decrease in NK cell percentages (Table 3). Regarding cytokine responses to persistent HCV infection, past reports in diversified patient groups were rather inconsistent: enhanced T_H1 responses [26–29], T_H2 responses [30–32], or both types [33,34]. Although differing degrees of pathogenesis and/or inflammation among study patient groups may be in part responsible for this discrepancy [34,35], some potential methodological drawbacks in studies demonstrating T_H2 cytokine predominance were indicated [27]. The present study on lymphocyte subsets suggested enhanced T_H1 immunity in persistent HCV infection, supporting a view that enhanced T_H1 immunity alone is not sufficient to regulate the virus in many cases of HCV infection.

As observed in this study, both decreased and increased percentages of peripheral NK cells and total CD8 T cells, respectively, have been reported in HCV persistent individuals [36–39]. A reduction in NK cells is assumed to be linked to ongoing viremia that may induce continuous proliferation of CD8 T cells. A recent study on murine cytomegalovirus infection indicated that NK cells negatively regulated the number and activity of virus-specific CD8 T cells as well as CD4 T cells that played a critical role in limiting viral persistence; lack of NK cell activation resulted in increased numbers of CD8 T and CD4 T cells along with enhanced effector functions through antigen presentation by viral-infected antigen-presenting cells [40]. Such functional interplay among NK cells, antigen-presenting cells, and CD8 T cells may be common in virally infected hosts. It is also plausible that reduced NK cells of individuals may in part reflect their weakened natural immunity upon HCV infection, preferentially leading to failure of HCV-infected cell clearance [41].

Finally, our follow-up survey of the HCV persistence group indicated that increased T_H1 cell percentages were associated with accelerated progression of liver fibrosis, whereas T_C1 and NK cell percentages were inversely associated with progression (Table 4). In accordance with preceding studies [26,28,42], this study demonstrates that T_H1 immunity plays a vital role in HCV-related fibrosis progression. In the liver as well as peripheral blood of individuals with chronic HCV infection, T_H1 cells may enhance CTL response and macrophage activation by producing cytokines, such as IL-2, IFN-γ, and tumor necrosis factor-α, thereby facilitating the necroinflammatory process of hepatitis C [26,42]. By contrast, increased T_C1 cell percentages in total CD8 T cells were associated with slower progression of fibrosis—new findings reported in this study. T_C1 cells express a chemokine receptor, CXCR3, which is required for migration to the HCV-infected liver [22], and we inferred that the increased T_C1 fraction includes HCV-specific CD8 T cells. Several studies have demonstrated relationships between higher numbers of circulating as well as intrahepatic HCV-specific CD8 T cells and lesser degrees of liver fibrosis during chronic HCV infection [43–46]. A plausible explanation is that HCV-specific CD8 T cells might control the virus without exerting cytotoxic effects on hepatocytes [46]. Alternatively, a population of CD8 T cells secreting an antifibrotic cytokine, IL-10, may be implicated in attenuation of hepatocyte killing and protection against liver injury [45,47].

A limitation of this study is that we examined clinical and immunologic data only from peripheral blood. Intrahepatic lymphocytes are assumed to have features distinct from those in peripheral blood [48]. Also, our comparison of lymphocyte subsets among study groups was cross-sectional, making it difficult to identify immunologic factors responsible for persistent HCV infection.

In conclusion, this study identified immunologic characteristics associated with HCV infection in a Japanese population and also indicated that peripheral T_H1, T_C1, and NK cell subsets will be useful for predicting progression of hepatitis in persistently HCV-infected patients and consequent development of hepatocellular carcinomas.

Acknowledgments

The Radiation Effects Research Foundation (RERF), Hiroshima and Nagasaki, Japan, is a private, nonprofit foundation funded by the Japanese Ministry of Health, Labor, and Welfare and the U.S. Department of Energy, the latter in part through the National Academy of Sciences. This research was based on RERF Research Protocols 3-09, 4-02, 2-00, and 9-92 and was supported in part by the U.S. National Institute of Allergy and Infectious Diseases (NIAID Contract HHSN272200900059C).

Appendix. Supplementary data

Supplementary data associated with this article can be found, in the online version, at doi:10.1016/j.humimm.2011.05.029.

References

[1] Shepard CW, Finelli L, Alter MJ. Global epidemiology of hepatitis C virus infection. Lancet Infect Dis 2005;5:558–67.
[2] Fung J, Lai CL, Yuen MF. Hepatitis B and C virus-related carcinogenesis. Clin Microbiol Infect 2009;15:964–70.
[3] Post J, Ratnarajah S, Lloyd AR. Immunological determinants of the outcomes from primary hepatitis C infection. Cell Mol Life Sci 2009;66:733–56.
[4] Sklan EH, Charuworn P, Pang PS, Glenn JS. Mechanisms of HCV survival in the host. Nat. Rev Gastroenterol Hepatol 2009;6:217–27.
[5] Crotta S, Stilla A, Wack A, D'Andrea A, Nuti S, D'Oro U, et al. Inhibition of natural killer cells through engagement of CD81 by the major hepatitis C virus envelope protein. J Exp Med 2002;195:35–41.
[6] Nattermann J, Nischalke HD, Hofmeister V, Ahlenstiel G, Zimmermann H, Leifeld L, et al. The HLA-A2 restricted T cell epitope HCV core 35-44 stabilizes HLA-E expression and inhibits cytolysis mediated by natural killer cells. Am J Pathol 2005;166:443–53.
[7] Piasecki BA, Lewis JD, Reddy KR, Bellamy SL, Porter SB, Weinrieb RM, et al. Influence of alcohol use, race, and viral coinfections on spontaneous HCV clearance in a US veteran population. Hepatology 2004;40:892–9.
[8] Stämpfli MR, Anderson GP. How cigarette smoke skews immune responses to promote infection, lung disease and cancer. Nat Rev Immunol 2009;9:377–84.
[9] Kusunoki Y, Hayashi T. Long-lasting alterations of the immune system by ionizing radiation exposure: implications for disease development among atomic bomb survivors. Int J Radiat Biol 2008;84:1–14.
[10] Ellenberg JH, Nelson KB. Sample selection and the natural history of disease. Studies of febrile seizures. JAMA 1980;243:1337–40.
[11] Beebe GW, Fujisawa H, Yamasaki M. Adult Health Study Reference Papers, A: Selection of the Sample, and B: Characteristics of the Sample. Technical Report 10-60. Hiroshima: Atomic Bomb Casualty Comission; 1960.
[12] Fujiwara S, Kusumi S, Cologne J, Akahoshi M, Kodama K, Yoshizawa H. Prevalence of anti-hepatitis C virus antibody and chronic liver disease among atomic bomb survivors. Radiat Res 2000;154:12–9.
[13] Ono E, Shiratori Y, Okudaira T, Imamura M, Teratani T, Kanai F, et al. Platelet count reflects stage of chronic hepatitis C. Hepatol Res 1999;15:192–200.
[14] Pohl A, Behling C, Oliver D, Kilani M, Monson P, Hassanein T. Serum aminotransferase levels and platelet counts as predictors of degree of fibrosis in chronic hepatitis C virus infection. Am J Gastroenterol 2001;96:3142–6.
[15] Coverdale SA, Samarasinghe DA, Lin R, Kench J, Byth K, Khan MH, et al. Changes in antipyrine clearance and platelet count, but not conventional liver tests, correlate with fibrotic change in chronic hepatitis C: value for predicting fibrotic progression. Am J Gastroenterol 2003;98:1384–90.
[16] Moriyama M, Matsumura H, Aoki H, Shimizu T, Nakai K, Saito T, et al. Long-term outcome, with monitoring of platelet counts, in patients with chronic hepatitis C and liver cirrhosis after interferon therapy. Intervirology 2003;46:296–307.
[17] Kawasaki T, Takeshita A, Souda K, Kobayashi Y, Kikuyama M, Suzuki F, et al. Serum thrombopoietin levels in patients with chronic hepatitis and liver cirrhosis. Am J Gastroenterol 1999;94:1918–22.
[18] Olariu M, Olariu C, Olteanu D. Thrombocytopenia in chronic hepatitis C. J Gastrointest Liver Dis 2010;19:381–5.
[19] Cullings HM, Fujita S, Funamoto S, Grant EJ, Kerr GD, Preston DL. Dose estimation for atomic bomb survivor studies: its evolution and present status. Radiat Res 2006;166:219–54.
[20] Sallusto F, Lenig D, Mackay CR, Lanzavecchia A. Flexible programs of chemokine receptor expression on human polarized T helper 1 and 2 lymphocytes. J Exp Med 1998;187:875–83.
[21] Cosmi L, Annunziato F, Galli MIG, Maggi RME, Nagata K, Romagnani S. CRTH2 is the most reliable marker for the detection of circulating human type 2 Th and type 2 T cytotoxic cells in health and disease. Eur J Immunol 2000;30:2972–9.

[22] Larrubia JR, Calvino M, Benito S, Sanz-de-Villalobos E, Perna C, Perez-Hornedo J, et al. The role of CCR5/CXCR3 expressing CD8+ cells in liver damage and viral control during persistent hepatitis C virus infection. J Hepatol 2007;47:632–41.
[23] Yamaoka M, Kusunoki Y, Kasagi F, Hayashi T, Nakachi K, Kyoizumi S. Decreases in percentages of naïve CD4 and CD8 T cells and increases in percentages of memory CD8 T-cell subsets in the peripheral blood lymphocyte populations of A-bomb survivors. Radiat Res 2004;161:290–8.
[24] Armitage P, Berry G, Matthews JNS. Statistical Methods in Medical Research (4th ed). Oxford: Blackwell Scientific; 2002.
[25] Hayashi T, Morishita Y, Kubo Y, Kusunoki Y, Hayashi I, Kasagi F, et al. Long-term effects of radiation dose on inflammatory markers in atomic bomb survivors. Am J Med 2005;118:83–6.
[26] Napoli J, Bishop GA, McGuinness PH, Painter DM, McCaughan GW. Progressive liver injury in chronic hepatitis C infection correlates with increased intrahepatic expression of Th1-associated cytokines. Hepatology 1996;24:759–65.
[27] Bergamini A, Bolacchi F, Cerasari G, Carvelli C, Faggioli E, Cepparulo M, et al. Lack of evidence for the Th2 predominance in patients with chronic hepatitis C. Clin Exp Immunol 2001;123:451–8.
[28] Sobue S, Nomura T, Ishikawa T, Ito S, Saso K, Ohara H, et al. Th1/Th2 cytokine profiles and their relationship to clinical features in patients with chronic hepatitis C virus infection. J Gastroenterol 2001;36:544–51.
[29] Gigi E, Raptopoulou-Gigi M, Kalogeridis A, Masiou S, Orphanou E, Vrettou E, et al. Cytokine mRNA expression in hepatitis C virus infection: TH1 predominance in patients with chronic hepatitis C and TH1–TH2 cytokine profile in subjects with self-limited disease. J Viral Hepat 2008;15:145–54.
[30] Reiser M, Marousis CG, Nelson DR, Lauer G, González-Peralta RP, Davis GL, et al. Serum interleukin 4 and interleukin 10 levels in patients with chronic hepatitis C virus infection. J Hepatol 1997;26:471–8.
[31] Fan XG, Liu WE, Li CZ, Wang ZC, Luo LX, Tan DM, et al. Circulating Th1 and Th2 cytokines in patients with hepatitis C virus infection. Mediat Inflamm 1998;7:295–7.
[32] Abayli B, Canataroğlu A, Akkiz H. Serum profile of T helper 1 and T helper 2 cytokines in patients with chronic hepatitis C virus infection. Turk J Gastroenterol 2003;14:7–11.
[33] Cacciarelli TV, Martinez OM, Gish RG, Villanueva JC, Krams SM. Immunoregulatory cytokines in chronic hepatitis C virus infection: pre- and posttreatment with interferon alfa. Hepatology 1996;24:6–9.
[34] Kakumu S, Okumura A, Ishikawa T, Yano M, Enomoto A, Nishimura H, et al. Serum levels of IL-10, IL-15 and soluble tumour necrosis factor-alpha (TNF-alpha) receptors in type C chronic liver disease. Clin Exp Immunol 1997;109:458–63.
[35] Anthony DD, Post AB, Valdez H, Peterson DL, Murphy M, Heeger PS. ELISPOT analysis of hepatitis C virus protein-specific IFN-gamma-producing peripheral blood lymphocytes in infected humans with and without cirrhosis. Clin Immunol 2001;99:232–40.
[36] Chan TM, Ho SK, Lai CL, Cheng IK, Lai KN. Lymphocyte subsets in renal allograft recipients with chronic hepatitis C virus infection. Nephrol Dial Transplant 1999;14:717–22.
[37] Chang KM, Thimme R, Melpolder JJ, Oldach D, Pemberton J, Moorhead-Loudis J, et al. Differential CD4(+) and CD8(+) T-cell responsiveness in hepatitis C virus infection. Hepatology 2001;33:267–76.
[38] Pár G, Rukavina D, Podack ER, Horányi M, Szekeres-Barthó J, Hegedüs G, et al. Decrease in CD3-negative-CD8dim(+) and Vdelta2/Vgamma9 TcR+ peripheral blood lymphocyte counts, low perforin expression and the impairment of natural killer cell activity is associated with chronic hepatitis C virus infection. J Hepatol 2002;37:514–22.
[39] Morishima C, Paschal DM, Wang CC, Yoshihara CS, Wood BL, Yeo AE, et al. Decreased NK cell frequency in chronic hepatitis C does not affect ex vivo cytolytic killing. Hepatology 2006;43:573–80.
[40] Andrews DM, Estcourt MJ, Andoniou CE, Wikstrom ME, Khong A, Voigt V, et al. Innate immunity defines the capacity of antiviral T cells to limit persistent infection. J Exp Med 2010;207:1333–43.
[41] Golden-Mason L, Cox AL, Randall JA, Cheng L, Rosen HR. Increased natural killer cell cytotoxicity and NKp30 expression protects against hepatitis C virus infection in high-risk individuals and inhibits replication in vitro. Hepatology 2010;52:1581–9.
[42] Moura AS, Carmo RA, Teixeira AL, Leite VH, Rocha MO. Soluble inflammatory markers as predictors of liver histological changes in patients with chronic hepatitis C virus infection. Eur J Clin Microbiol Infect Dis 2010;29:1153–61.
[43] Sreenarasimhaiah J, Jaramillo A, Crippin J, Lisker-Melman M, Chapman WC, Mohanakumar T. Lack of optimal T-cell reactivity against the hepatitis C virus is associated with the development of fibrosis/cirrhosis during chronic hepatitis. Hum Immunol 2003;64:224–30.
[44] Cardoso EM, Duarte MA, Ribeiro E, Rodrigues P, Hultcrantz R, Sampaio P, et al. A study of some hepatic immunological markers, iron load and virus genotype in chronic hepatitis C. J Hepatol 2004;41:319–26.
[45] Abel M, Sène D, Pol S, Bourlière M, Poynard T, Charlotte F, et al. Intrahepatic virus-specific IL-10-producing CD8 T cells prevent liver damage during chronic hepatitis C virus infection. Hepatology 2006;44:1607–16.
[46] Bonilla N, Barget N, Andrieu M, Roulot D, Letoumelin P, Grando V, et al. Interferon gamma-secreting HCV-specific CD8+ T cells in the liver of patients with chronic C hepatitis: relation to liver fibrosis—ANRS HC EP07 study. J Viral Hepatol 2006;13:474–81.
[47] Accapezzato D, Francavilla V, Paroli M, Casciaro M, Chircu LV, Cividini A, et al. Hepatic expansion of a virus-specific regulatory CD8(+) T cell population in chronic hepatitis C virus infection. J Clin Invest 2004;113:963–72.
[48] Grabowska AM, Lechner F, Klenerman P, Tighe PJ, Ryder S, Ball JK, et al. Direct ex vivo comparison of the breadth and specificity of the T cells in the liver and peripheral blood of patients with chronic HCV infection. Eur J Immunol 2001;31:2388–94.

Mutation Research 721 (2011) 101–107

Contents lists available at ScienceDirect

Mutation Research/Genetic Toxicology and Environmental Mutagenesis

journal homepage: www.elsevier.com/locate/gentox
Community address: www.elsevier.com/locate/mutres

Easy detection of GFP-positive mutants following forward mutations at specific gene locus in cultured human cells

Asao Noda [a,*], Yuko Hirai [a], Yoshiaki Kodama [a], Warren W. Kretzschmar [a], Kanya Hamasaki [a], Yoichiro Kusunoki [b], Hiroshi Mitani [c], Harry M. Cullings [d], Nori Nakamura [a]

[a] Department of Genetics, Radiation Effects Research Foundation, 5-2 Hijiyama Park, Minami-Ku, Hiroshima 732-0815, Japan
[b] Departments of Radiobiology and Molecular Epidemiology, Radiation Effects Research Foundation, 5-2 Hijiyama Park, Minami-Ku, Hiroshima 732-0815, Japan
[c] Department of Integrated Biosciences, Graduate School of Frontier Sciences, The University of Tokyo, Kashiwa-no-ha 5-1-5, Kashiwa, Chiba 277-8572, Japan
[d] Department of Statistics, Radiation Effects Research Foundation, 5-2 Hijiyama Park, Minami-Ku, Hiroshima 732-0815, Japan

ARTICLE INFO

Article history:
Received 5 October 2010
Received in revised form
19 November 2010
Accepted 29 December 2010
Available online 6 January 2011

Keywords:
Radiation
Tet repressor
Tet operator
GFP
HPRT

ABSTRACT

We have generated a new mutation assay system using HT1080 human fibrosarcoma cells, which consists of a combination of tetracycline-operator dependent *GFP* gene (*TetO-EGFP*) and tetracycline repressor (*TetR*) genes, where the expression of *GFP* gene is under strict control of TetR protein, and the *TetR* gene is located within the endogenous *HPRT* gene. In this system, any inactivating mutation at the *TetR* gene or large deletions including the gene itself results in high expression of *GFP* gene (>200-fold increase) in the cells, which can be readily scored not only by a flow cytometer but also under a fluorescent microscope. With this new cell line, we show that the spontaneous mutation rate at the *TetR* locus was $2.8–3.4 \times 10^{-6}$/cell division, slightly lower than the rate at the endogenous *HPRT* gene of HT1080 cells, and has a dose response to X rays as a mutagen. We also isolated variant clones with elevated spontaneous mutation rate (i.e., genetically unstable cells) following X irradiation. Spontaneous GFP-positive mutants were predominantly base-change mutations at the *TetR* gene while those obtained after X irradiation often contained large deletions which spanned up to 6 Mb. The results indicate that the bacterial TetR/TetO regulatory units work extremely well as a mutation detection system in human cells, and any part of the human genome may be tested for mutation sensitivity following targeted insertion of the *TetR* gene in a stably expressing gene.

1. Introduction

Quite a large number of chemicals are newly produced every year and it is desired that genotoxic chemicals are effectively excluded from our living environment as they are potentially carcinogenic. Such an effort is important for living in a safe environment. Accordingly, screening of a large number of environmental mutagens has been conducted using bacteria and cultured mammalian cells [1,2].

In cultured mammalian cells, mutation detection systems use primarily genes involved in salvage pathways of nucleic acid synthesis (the genes are non-essential for cell survival); namely, *HPRT* and *TK* genes. Normal cells die in the presence of cytotoxic analogues (6-thioguanine or trifluorothymidine, respectively) by incorporating them into nucleic acids, while mutant cells deficient in the enzyme activity cannot utilize the analogue and survive as they use *de novo* pathways for the nucleic acid synthesis [3,4]. In those systems, cells treated with test chemicals have to be subcultured for a few days to nearly 1 week for the full expression of the mutant phenotype before being subjected to colony formation in selective media, a step that takes an additional 1–2 weeks. Thus, a total of 2–3 weeks are required for one set of experiments.

There are also *in vivo* systems which utilize naturally available mutant alleles of mice; namely, pink eye unstable (p^{un}) in retina and coat hair [5], and *Dlb-1* in colon [6]. Expression of those genes is restricted to specific tissues, however, which limits the usefulness of the systems as a tool for screening environmental mutagens. Other *in vivo* systems utilize *Hprt*, and animals heterozygous for the endogenous *Tk* and *Aprt* genes as reporters. All share the limitation of only being performed in a small number of cell types, such as T lymphocytes and skin fibroblasts.

More recently, developments of molecular biology techniques have added new options to create systems with foreign reporter genes for mutagenesis studies. One class of such systems consists of a gene originating from prokaryotes that is inserted into the mammalian genome. Following mutagen treatment, DNA is recovered and mutations are quantified and analyzed in *Escherichia coli* [7]. Several different strains of transgenic animals using such a

* Corresponding author. Tel.: +81 82 261 3131; fax: +81 82 263 7279.
E-mail addresses: asnoda@rerf.or.jp, gk7a-nd@asahi-net.or.jp (A. Noda).

1383-5718/$ – see front matter © 2011 Elsevier B.V. All rights reserved.
doi:10.1016/j.mrgentox.2010.12.010

system have also been produced [8]. The second class is a mutation detection system in which mutations are more easily detected *in situ* in genetically altered cells which carry a transgene, most frequently green fluorescence protein (*GFP*) gene. In such a system, the reporter gene is set as not to express under normal conditions, but to express following mutagenesis. For example, in a system consisting of a tandem array of two *GFP* genes each of which contains mutations at different sites, gene conversion-type events primarily give rise to an intact *GFP* gene [9–14]. In another system consisting of *GFP* genes which were purposely set as out of reading frame by an insertion of micro-repeat sequences at its 5′ side, deletion of restricted numbers of bases can make the gene in frame and the cells will fluoresce [15,16]. Transgenic animals are also created [10]. The major constraint of those assays is that only specific types of mutational events are detectable. And obviously, it is not possible to detect large deletions including the reporter gene and the neighboring segments of DNA (e.g., 1 Mb deletions), frequent events following exposure to ionizing radiations.

Therefore, for detection of both base substitutions and large deletions, a reversion system cannot satisfy the conditions but a component of a forward mutation system needs to be included. We propose that a possible system is a compound two-gene system comprised suppressor and effector genes. Dobrovolsky et al. [17] previously used a compound system consisting of tetracycline-inducible repressor (*TetR*) gene and *GFP* gene, the latter is under the control of tetracycline-operator (*TetO-GFP*). They reported, however, that the suppressive function of the *TetR* gene was not effective enough and it was difficult to distinguish mutants from cells with intermediate levels of GFP expression, probably due to multiple copies of the integrated *GFP* genes and/or epigenetic modification of the *TetR* gene. Consequently, the system is not easy to use as a mutation-screening system. In the present study, we have overcome the problems using a single copy integration of *GFP* gene and targeted insertion of the *TetR* gene into intron 3 of the endogenous *HPRT* gene, which is known to be ubiquitously expressed. With the new system, it is now possible to measure any inactivating mutations (forward mutations) in the target *TetR* gene by means of flow-cytometry. We can measure not only spontaneous mutation rates, but also mutagenic effects of large and small doses of ionizing radiation. Applications of the system to an *in vivo* system will also be discussed.

2. Materials and methods

2.1. Cells and culture conditions

Human fibrosarcoma cell line HT1080 (ATCC No. CCL121), carrying a nearly normal karyotype (44+XY; [18]), was used throughout the study. The cells were maintained under standard culture conditions (MEM with Earl's salts supplemented with 10% FCS), and antibiotics G418 (400 μg/ml), blasticidin (5 μg/ml), or tetracycline (1 μg/ml), was added when necessary. To isolate HPRT proficient or deficient cells, HAT (1 × HAT) or 6TG (2.5 μg/ml)-containing medium was used for the respective selection. X-irradiation was carried out with a Shimadzu X-irradiator (220 kV, 8 mA with 0.5 mm Al and 0.3 mm Cu filters) with a dose rate of about 0.34 Gy/min. For flow-cytometric analyses, cells were treated with trypsin–EDTA, and were suspended in PBS containing 1% FCS at about 10^6 cells/ml. Samples were analyzed by a flow cytometer or a cell sorter (FACScan; Becton, NJ or JSAN; Bay Bioscience, Kobe) by gating single cells.

2.2. Plasmid construction and gene targeting (Supplementary figures)

2.2.1. Tetracycline operator (TetO)-driven EGFP vector

EGFP gene fragment (0.8 kb) was excised from plasmid pEGFP-C1 (Clonetech) by *Eco*47III and *Sma*I digestion, and ligated with *Eco*RV digested pcDNA4/TO (Invitrogen) which carries CMV promoter in conjunction with tandem duplicated Tet operator sequences (2 × TetO). The resulting plasmid, pTetO-GFP#16, was linearized by partial digestion with *Hin*dIII, and ligated with a *Hin*dIII-digested bsr fragment (0.5 kb) from pSV2bsr (Funakoshi) to make plasmid pTetO-GFPbsr#45. The plasmid was then digested with *Apa*I and recircularized to remove unnecessary sequences (*Xho*I site) flanked with the 3′ side of bsr. The resulting plasmid (pTetO-GFPbsr#45-(-Xho)#15) was digested with *Xho*I, filled-in and religated to make GFP-bsr fusion gene (plasmid pTetO-EGFPbsr#1). The plasmid was linearized by digestion with *Ssp*I, and electroporated into HT1080 cells using standard pulse settings for adherent cells (25 μF, 1000 V). Colonies resistant to blasticidin were recovered and propagated. Intensity of GFP fluorescence was measured in order to select clones that exhibit strong and uniform GFP expression among the cells in that clone.

2.2.2. HPRT gene targeting vector

A 8.4 kb of genomic DNA fragment containing human *HPRT* exons 2 and 3 (left arm of the targeting vector) was isolated from the human BAC clone (bWXD187, AC004387) by *Eco*RI digestion [18] and was inserted into the *Eco*RI site of the pBS(SKII) plasmid. The resulting plasmid was digested with *Eco*RV, and ligated with blunted DNA fragment containing a CMV promoter-Tet repressor (*TetR*) gene unit [a 2.3 kb of *Mlu*I fragment from the plasmid pcDNA6/TR (Invitrogen), where both *Mlu*I ends were filled-in], resulting in the plasmid p8.4-6TR#2. Next, 2.3 kb of DNA fragment (right arm of targeting vector), derived from *Eco*RI-digest of human *HPRT* intron 3, was inserted into *Eco*RI digested pBS(SKII) to make plasmid pBS2.3#3. Then 1.2 kb of the loxP-neo gene fragment was excised from pBS-MCneo [18] by *Sma*I and *Hin*cII digestion, and ligated with *Sma*I-digested pBS2.3#3 to make plasmid p2.3neo#1. To exclude cells that have undergone untargeted integration of the vector (random insertion in the genome), a 1.1 kb of *DTA* gene fragment which encodes diphtheria toxin [19] and is derived from *Eco*RV and *Hin*cII digestion of pBS-MC1DTA, was also inserted into blunted-*Sal*I site of p2.3neo#1 to give the plasmid p2.3neoDTA#2. Then, a 4.6 kb of neo-2.3kb-DTA fragment was excised from p2.3neoDTA#2 by *Sma*I and *Apa*I digestion, filled-in, and then inserted into blunted-*Sal*I site of the plasmid p8.4-6TR#2 to give the targeting plasmid, pHPRT-6TRtarget#6.

2.2.3. Targeted integration of CMV TetR-floxed neo gene fragment into endogenous HPRT gene locus

The 15.4 kb of the targeting fragment from the vector (HPRT-6TR fragment) was isolated with *Bss*HII digestion, and electroporated into the selected cell clones obtained from the above-mentioned step (2.2.1), whose GFP expression was highest. Among the G418 resistant clones recovered, those which underwent correct integration of the HPRT-6TR fragment into endogenous *HPRT* gene through homologous recombination were identified by PCR and Southern analyses (Fig. 1). As expected, those clones showed no *GFP* gene expression through silencing by TetR protein.

2.3. Detection of mutant cells

Any loss-of-function mutation at the *TetR* gene located in the *HPRT* locus, irrespective of point mutations or deletions encompassing the integrated *TetR* sequences, releases the *GFP* gene expression from silencing. Adding tetracycline (1 μg/ml) into the culture media can simulate this release. Presumed *TetR* mutant cells were defined as having GFP levels equivalent to those of tetracycline-treated cells. This equivalency of GFP expression was confirmed by flow cytometry. We defined mutants as cells displaying elevated levels of fluorescence intensity of GFP by at least 200-fold compared with the level of autofluorescence of wild-type or untreated cells (Fig. 2A)

2.4. Mutation assay

Clonal cell populations propagated from a single cell were grown up to 4.5×10^7 cells, and were then cryopreserved in 10 ampoules (4.5×10^6 cells each). Each ampoule was thawed and used for each set of mutagenesis experiments so that the background mutation frequency should remain low and constant. The frequency of GFP-positive mutant cells was measured by a flow cytometer (FACScan, Becton-Dickinson) by screening at least 10^6 cells per sample. In low dose experiments (Fig. 4C), 10^7 cells were subjected for each measurement.

2.5. Isolations and characterizations of mutant cells by multiplex PCR

Mutant cells that arose in the cultures of unirradiated or irradiated cells were detected and isolated with a desk-top cell sorter, JSAN. Each mutant was isolated and propagated up to 2×10^6 cells, and their genomic DNA was extracted. Multiplex PCR (Qiagen kit) was carried out to amplify *HPRT* exons 1–9 as well as integrated *TetR* gene in a single tube. Primers used are: HPRT exon 1 (TGGGACGTCTGGTCCAAGGATTCA, CCGAACCCGGGAAACTGGCCGCCC), exon 2 (CACCTAAATTTCTCTGATAGACTAAGG, GATACTAAGTAATTAGTAAGGCC), exon 3 (GTGGAAGTTTAATGACTAAGAG, GTATATATCCTCCAAGGTGACTAG), exon 4 (GCTATGGATATTAGCTAGCTAAC, GCTTCCAAGGGTTAAATAACCCA), exon 5 (AGCATCTAAAAACAAGAGTTTGG, AACTGATGCAGAGGAATTTCTCTC), exon 6 (GATTTTGGTGAGAATTACTGTGCTG, CACTTAATCCCCCTTCAAATGAG), exons 7+8 (ACCAAGTGCCTTGTCTGTAGTGTC, TCCTAAATCTTCCTCAACCATGTTC), exon 9 (ACTAATGTGATAGACTACTGC, GAACTGCTGACAAAGATTCACTG), TetR (AGGGCGAATTGATATGTCTAGA, GCTGCAATAAACAAGTTCTGCT) [20].

For genome walking with STS PCR, we set STS primers at about 1 Mb intervals from both sides of the *HPRT* gene locus, and multiplex PCR with different combinations of 15 STS sites was carried out to reveal the deletion size of the DNA sequences around *HPRT* (*TetR*) gene locus. For those mutants with no evidence of deletion of

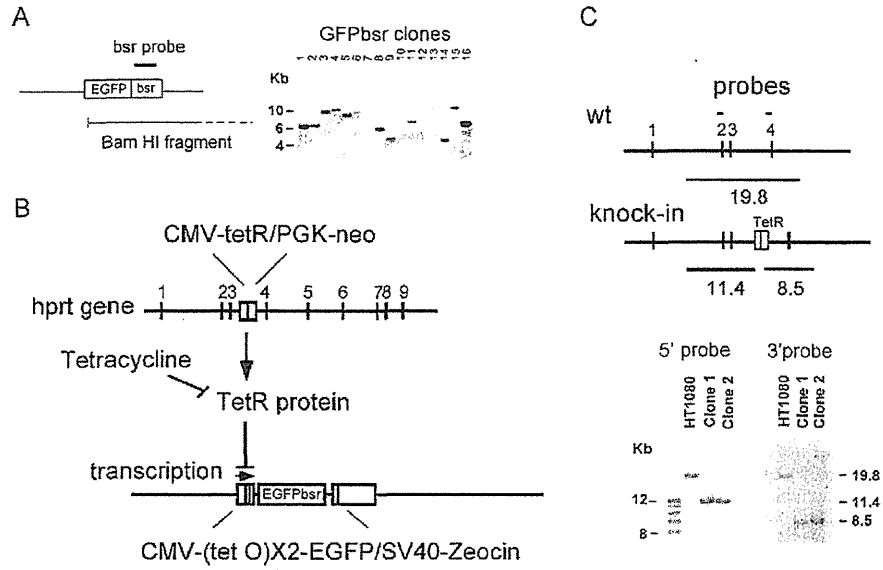

Fig. 1. Generation of GFP transgenic/TetR knock-in HT1080 cells. (A) Integration of a single copy of a vector carrying the TetO-EGFPbsr sequence. The left picture indicates locations of the bsr probe and *Bam*HI site, and the right panel shows the results of Southern blots of 16 transfectants. (B) Diagram illustrating the intracellular system in which GFP transcription is induced by inactivation of *TetR* gene which was inserted in intron 3 of *HPRT* gene by targeted insertion, or by inhibition of TetR protein with tetracycline. (C) Verification of targeted integration of *TetR* gene. DNA from the candidate clones were digested with *StuI* and hybridized with 5′ or 3′ probes, respectively. Locations of the probes and fragments to be detected are indicated. In wild-type cells both probes detected the 19.8 kb band, while in knock-in cells 5′ and 3′ probes detected the 11.4 and 8.5 kb bands, respectively.

any *HPRT* exon, *TetR* gene was amplified by PCR and sequenced to determine the site of point mutations.

2.6. Measurements of mutant frequency and estimation of spontaneous mutation rate

One ampoule was thawed and 4×10^6 cells were used to initiate a culture. Every 3–4 days, cell number as well as mutant cell frequency were determined and 4×10^6 cells were taken anew to continue the culture. The experiments were repeated twice (this is termed as "large-scale inoculation and short-term culture").

The spontaneous mutation rate was calculated as reported by Nadas et al. [21,22] and Foster [23]. In brief, we assumed that only one of the two daughter cells becomes mutant following a spontaneous mutation in a cell cycle because most of the spontaneous mutations are base-change mutations and hence would affect only one strand of the DNA double strands. Assume that there are m mutant cells preexisting in a

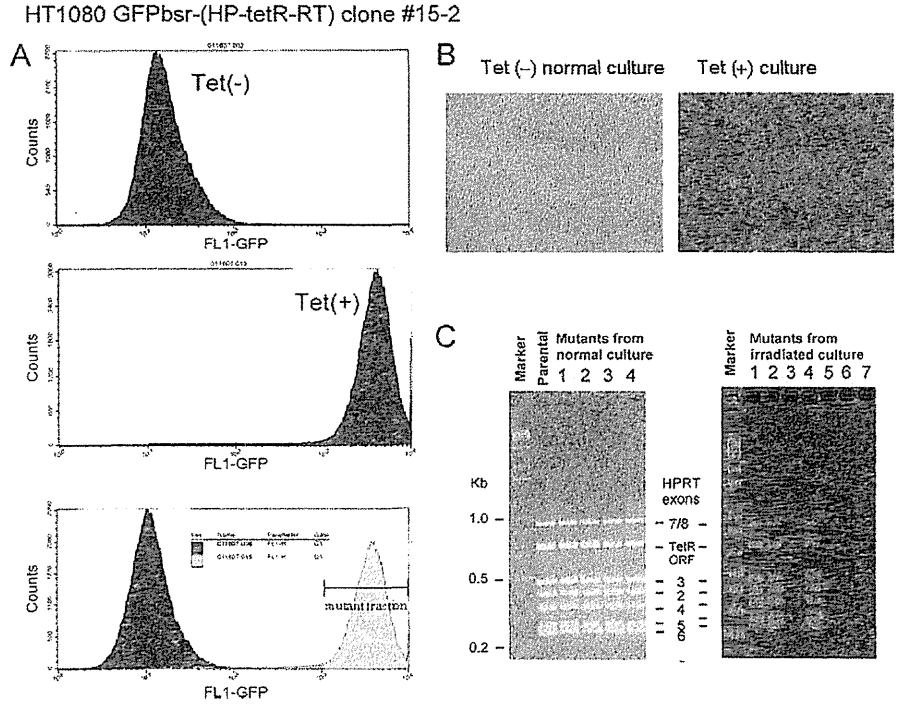

Fig. 2. Tet On/Off system verifications and analyses of spontaneous and radiation-related mutants. (A) Flow cytometric analyses of HT1080 cells bearing the TetR/TetO-GFP system cultured overnight in the absence [Tet(−), upper panel] or the presence of tetracycline [Tet(+), middle panel]. The lower panel indicates the window for mutant detection (the mean fluorescent intensity is >250-fold higher than in normal cells). (B) Two representative views under fluorescent microscopy (×100). (C) Molecular analyses of mutant clones for the presence or absence of *HPRT* exons and *TetR* gene by multiplex PCR. All spontaneous mutants retained the 7 exons whereas four out of seven mutants recovered after radiation exposure had lost all of them.

starting population consisting of n_0 cells and the population reaches n_1 at the end of the culture, which took a generations; namely, $n_1 = n_0 \times 2^{a-1}$.

In such a growing cell population, new mutants arise in proportion to the number of cells that divide. Thus, at ith generation, the number of cells that divide is $n_0 \times 2^{i-1}$, and hence the number of new mutants is $p(n_0 \times 2^{i-1})$, where p stands for the spontaneous mutation rate. Since these mutants continue to divide until the population reaches ath generation, the number of mutants increases by $2^{(a-i)}$. That is, each generation equally contributes to produce spontaneous mutants by $p(n_0 \times 2^{i-1}) \times 2^{(a-i)} = p(n_0 \times 2^{a-1})$, and hence the total number of new mutants is $p(n_0 \times 2^{a-1}) \times a$ when the cell number reaches n_1.

In practice, let the mutant frequency measured at the start and the end of the culture be Mf_0 and Mf_1. Mf_1 is described as a function of the preexisting mutants plus new mutants that arose during this culture period, namely, $Mf_1 = m/n_0 + [p(n_0 \times 2^{a-1}) \times a/(n_0 \times 2^{a-1})]$. Since $Mf_0 = m/n_0$, the net increase of the mutant frequency is;

$$Mf_1 - Mf_0 = \left[\frac{p(n_0 \times 2^{a-1}) \times a}{(n_0 \times 2^{a-1})}\right] = pa \quad (1)$$

The classical Luria Delbrück fluctuation test was also conducted as previously reported except that, instead of using colony formation assay, mutant cell frequency was determined by flow cytometry. In brief, cells were inoculated at a low density, and 20–100 individual colonies were randomly isolated. Each colony was propagated to 2×10^6 cells, and the number of mutants in these cultures was determined. Mutation rates were calculated as follows:

$$r = aN \times \ln(NCa) \quad (2)$$

where r is the average number of mutants in each of the separately propagated cultures; a is the mutation rate; N is the number of cells in the expanded populations (2×10^6 in this case), and C is the number of clones examined [18,24].

For radiation mutagenesis experiments, 4×10^6 cell-aliquots were irradiated for each dose level, cultured for 6 days for the full expression of the mutant phenotype, and subjected to flow cytometric analysis to determine the mutant frequency.

2.7. Isolation of cell clones exhibiting genomic instability after X-irradiation

Three million cells were irradiated with 4 Gy, followed by a 5-day culture, trypsinized, and seeded at low densities. Then 400 individual colonies were randomly isolated and individually cultured in each well of 96-well plates until they reached confluence (about 2×10^4 cells/well). The number of mutants in individual wells was then counted under a fluorescent microscope. Wells containing more than 10 mutants were selected as candidate clones possibly harboring cells with genomic instability. Each clone was further propagated and examined for estimation of mutation rate with the "large-scale inoculation and short-term culture" method as well as the fluctuation test [24].

3. Results

3.1. Generation of cells bearing TetO-GFP gene which is under strict control by TetR gene

As mentioned in Section 1, the present study was aimed at creating a model system using a human cell line in which any inactivating mutations at *TetR*, including surrounding *HPRT* locus may be detected as GFP-positive cells. For this purpose, we used a compound system consisting of a combination of *TetR* and *TetO-GFP* genes.

In the first set of the experiments, cells were transfected with TetO-GFP-containing plasmids by chemical lipofection. However, all the blasticidin-resistant clones were found to contain multiple copies of the plasmid. Since we did not feel that this is a critical problem, we used those cells for targeted integration of *TetR* gene into the endogenous *HPRT* locus. About 30 candidate clones were isolated, but all of them showed variable frequencies of GFP-positive "mutant" cells at 10^{-4} to 10^{-3}, which seemed to be too high to be caused by true mutations. We speculated that this was probably because a single-copy *TetR* gene was insufficient to fully silence the expression of multicopied *TetO-GFP* genes, and decided to change the strategy to generate cells consisting of single copy integrations for both *TetR* and *TetO-GFP* genes.

For this purpose, we switched to use an electroporation technique in isolating GFP-positive and blasticidin-resistant clones, and found that the majority of the transfectants (~75%) contained a single copy of *TetO-GFP* gene (Fig. 1A). Subsequently, we isolated two clones (#3 and #15; Fig. 1A), which showed the brightest fluorescence intensity and carried a single copy of the gene, and used them as recipients for the second-step, targeted integration of the *TetR* gene into intron 3 of the *HPRT* gene also by electroporation. Among tens of thousands of G418 resistant colonies recovered, a few clones could be isolated which had undergone correct integrations of the *TetR* gene (Fig. 1B and C). We found that all the clones that had correct integration of *TetR* gene in the endogenous *HPRT* gene exhibited highly stable suppression of the *TetO-GFP* gene activity. It is noted that, although the *TetR* gene was integrated in a large intron 3, the normal function of the *HPRT* gene was destroyed and the cells became deficient in the HPRT activity (i.e., resistant to 6TG).

3.2. Flow cytometric analyses of the GFP-positive mutants

A high level of suppression of *TetO-GFP* gene activity by the expression of *TetR* gene was evident since, under normal culture conditions, no mutants were seen in most of the cell populations consisting of 5×10^5 cells, where each population originated from single cells. Further, the suppression was so profound that the expression level of GFP protein was increased by more than 200-fold upon inactivation of the TetR protein following treatment of the cells with tetracycline for overnight (*cf.* tet(−) and tet(+) panels in Fig. 2A). Since the lower limit of the fluorescence level specified for the GFP-positive cells is higher than the upper limit of the autofluorescence level of GFP-negative cells by one order of magnitude (Fig. 2A lower panel), we could clearly define the mutant window for GFP-positive cells as indicated with the crossbar. It is noted that the normal cells are not completely negative with regard to the fluorescence emission but show a low level of autofluorescence. Namely, the level of autofluorescence was 1.5–2.0 times higher in the parental cells (#15-2) compared with those in the original HT1080 cells. We noted that culturing the cells in the presence of commercially available, antibiotics-free FCS could diminish the level of autofluorescence, but this was not essential for the measurements of mutant frequencies. GFP-positive and -negative cells can also be clearly distinguished under a fluorescent microscope (Fig. 2B).

Before conducting quantitative measurements of radiation dose response, expression time course for mutant phenotype was monitored following exposure of 4×10^6 cells to 4 Gy of X rays. The results are shown in Fig. 3A and B, and indicated that 6 days, or 3 PDs, were required before the *TetR*-gene mutants fully express the GFP-positive phenotype, indicating that the degradation, or dilution by cell division, of pre-existed TetR proteins would determine the latency.

3.3. Spontaneous and radiation-induced mutations

Spontaneous mutation rate was estimated following repeated measurements of the mutant cell frequencies by flow cytometry during subcultures of a large cell population (5×10^6 cells). The results indicate that the mutant frequency increases in proportion to the increase in the number of population doublings (Fig. 4A). As the net increase of the mutant frequency is about $17/5 \times 10^5$ cells (or 3.4×10^{-5}) at 20 population doublings, the mean increase is 0.17×10^{-5}/population doubling, which gives an estimate of the spontaneous mutation rate as 0.34×10^{-5}/cell division from Eq. (1).

Results of the X-ray mutagenesis are shown in Fig. 4B and C. It appears that the dose response curve showed upward curvature (Fig. 4B), with linear-quadratic regression statistically significant ($p = 0.03$ for the term $(X - 1.5)^2$). Eye fitting of the data indicates that about 1 Gy can give rise to double the background mutation frequency. Low dose experiments were also conducted in a separate set of experiments, in which a larger number of

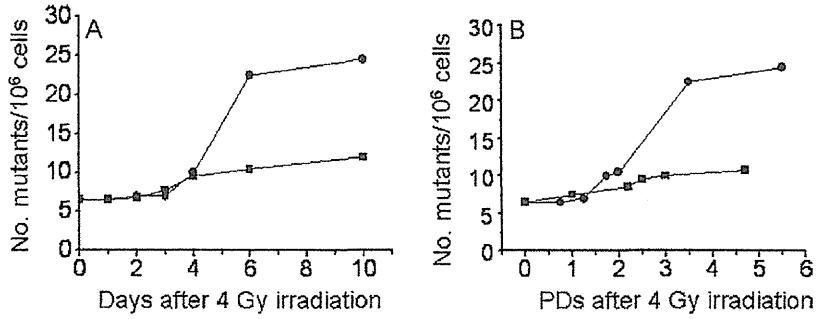

Fig. 3. Time course of mutant phenotype expression. Control and 4 Gy irradiated cells were serially cultured, and mutant frequencies were determined at the occasions of each split. ●, irradiated cells; ■, control cells. PDs: population doublings.

cells (10^7 cells) were irradiated and examined at each dose level since the radiation-related increase in the mutant frequency was expected to be much smaller. The results indicated a linear trend of dose response at a dose range of 50–400 mGy (Fig. 4C). Experiments at lower doses (below 50 mGy) were also conducted but the results were quite unstable.

3.4. Characterization of spontaneous and radiation-induced mutants

Mutants from irradiated or un-irradiated cultures were sorted using a JSAN cell sorter, and the mutant cells were grown individually in each well of 96-well microtiter plates to characterize the mutations at *HPRT* and *TetR* genes. Spontaneously arising mutants were obtained from large-scale untreated cultures of ~10^8 cells. Radiation-induced mutants were obtained from cultures of 6×10^6 cells irradiated with 4 Gy of X rays followed by a 6-day expression (the cell survival level following exposure to 4 Gy is ~20% by a colony assay in the parental cells). It was found that 10 spontaneous mutants were all normal with regard to the presence of 7 exons of *HPRT* gene and *TetR* gene (Fig. 2C left panel), and base sequencing study of four mutants showed that three bore base-change mutations and one had one-base deletion; namely, G to C mutation at base 260 (G260C), G283C, T231G, and deletion of one base at 649 (the numbers represent bases from the *TetR* start codon). All the point mutations caused amino acid substitution or premature stop. In contrast, among the mutants recovered from 4 Gy-irradiated cultures, only three out of seven retained the *HPRT* exons (Fig. 2C right panel, lanes 1, 2, and 4) and ultimately were found to carry base change mutations within the *TetR* gene (most likely originated from spontaneous events). The remaining four bore large-scale deletions encompassing 4–10 Mb including the entire *HPRT* locus as revealed by the results of multiplex PCR of *HPRT* exons (mutants 3, 5, 6, and 7) and genome walking with STS primers; specifically, mutants 3, 5, and 7 had deletions of ~4 Mb (and mutant 7 accompanied a complex rearrangement), and mutant 6 had a deletion of ~6 Mb.

3.5. Delayed effects of radiation

We examined whether the present system is able to detect radiation-induced genomic instability, which is expressed as an

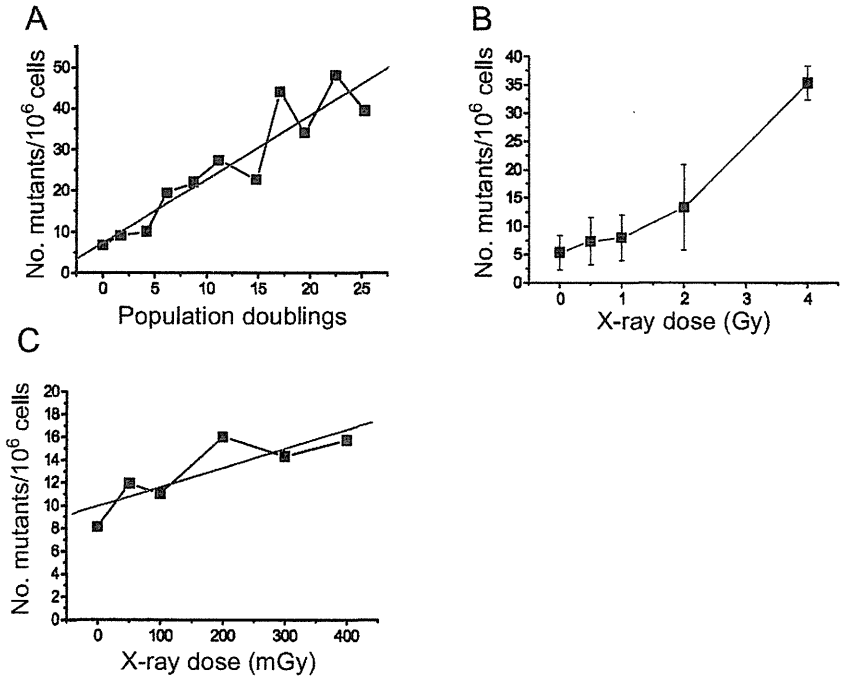

Fig. 4. Kinetics for the accumulation of spontaneous mutations, and dose response of radiation mutagenesis. (A) Mutant frequency at the time of each subculture was plotted against the number of population doublings. (B) X-ray dose response. Triplicate measurements were conducted at each dose level. (C) Radiation dose response at doses below 400 mGy.

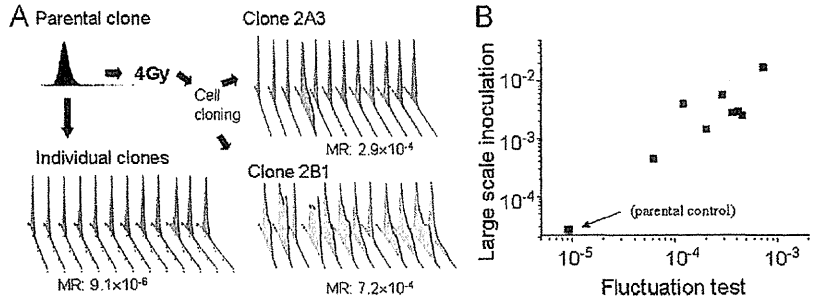

Fig. 5. Isolation of clones showing genomic instability following 4 Gy irradiation. (A) Cells were X-irradiated and 400 colonies were isolated in each well of 96-well microtiter plates. Candidate clones indicating genomic instability were screened under fluorescent microscopy. Spontaneous mutation rate was estimated either by "large-scale inoculation and short-term culture" method for the mass cultures of each clone or by the classic fluctuation test following further isolation of 12 colonies from each clone. In both cases, mutant frequency was measured by flow cytometry. The histograms shown for control cells and two clones 2A3 and 2B1, isolated after 4 Gy irradiation, indicate the frequency distribution of cells with different levels of fluorescence intensity. MR stands for the estimated mutation rate. (B) Comparison of the two mutation rates thus estimated.

enhanced mutation rate following radiation exposure. Three million cells were irradiated with 4 Gy of X rays, cultured for 6 days, and surviving cells were plated at low densities to isolate individual colonies. About 400 colonies were randomly isolated and cells from each clone were propagated in each well of 96-well plates until they reached confluence ($\sim 2 \times 10^4$/well). Then each well was examined with a fluorescent microscope to screen wells that contained more than 10 green cells as candidate clones exhibiting genomic instability. Given the spontaneous mutation rate is 2.8×10^{-6}/cell generation in the parental cells (#15-2 clone), the probability for a clonal cell population to yield 10 or more mutants among 2×10^4 cells is quite low.

In the initial screening, 22 candidate clones were isolated and mutation rates were measured using the "large-scale inoculation and short-term culture" method. Almost all the clones exhibited enhanced mutation rate except for four; namely, three had mutation rates lower than the parental ones and one was unable to be measured because of slow growth. Mutation rates showed a large variation from a relatively modest to extremely high levels; 6.0×10^{-5} to 2.0×10^{-2}/cell division. To compare the results with those by the classical fluctuation test, cells from typical candidate clones exhibiting modest to high mutation rates were inoculated at low densities and more than 10 colonies were randomly isolated and propagated to $\sim 2 \times 10^6$ cells, followed by flow-cytometric analyses to determine the mutant frequency. Whereas the fluctuation test of parental unirradiated #15-2 cells showed exactly the same mutant distribution profile in individual cell propagations, those of modestly unstable (2A3; 4×10^{-3}/cell division) and highly unstable clones (2B1; 2×10^{-2}/cell division) apparently produced abundant mutants when individual cells constituting the clone were propagated (Fig. 5A). Classical calculation (formula 2) gave rise to a mutation rate for parental cells of 9.1×10^{-6}, while 2A3 and 2B1 gave much higher rates, 2.9×10^{-4} and 7.2×10^{-4}/cell division, respectively. The results of the "large-scale inoculation and short-term culture" method were plotted against the results of fluctuation tests, which indicated a fairly good correlation between the two calculations (Fig. 5B). However, the large-scale inoculation method consistently showed higher rates than those obtained by the classic fluctuation tests, which could perhaps be partly due to a decreased colony-forming efficiency in highly unstable cells in the latter.

4. Discussion

The present assay system can detect a wide range of mutational events covering from base change mutations to megabase deletions, and does not require extensive processes and time necessary for colony formation of mutant cells (i.e., 1–2 weeks depending on the cells). That is a great advantage over the conventional mutation assays that require huge numbers of culture dishes as well as specific culture conditions. Thus the straightforward, flow cytometric analyses are promising future applications for general use. The only requirement is a 6-day post-irradiation subculture before determining the mutant frequency. Thus, the overall time for one set of experiments can be reduced from 2 to 3 weeks to one. It is unfortunate that the 6-day subculture (i.e., expression time) is still necessary, which is the same as that of the classic assay at the endogenous *HPRT* gene. It would be beneficial if the expression time could also be shortened by, say one half or 3–4 days. That is especially attractive for screening a large number of environmental chemicals for mutagenicity [25]. In that regard, dilution of the TetR proteins is the rate-limiting process and not the accumulation of GFP proteins, since only an overnight culture in the presence of tetracycline is sufficient for the full expression of GFP-positive phenotype (Fig. 2A) (tetracycline binds to the TetR protein and removes them from the TetO sequences by allosteric inhibition). Thus, to shorten the expression time, strategies to make the TetR proteins undergo faster turnover are needed; for example, genetic modification of the TetR protein to be more labile while maximally maintaining the binding capability to the TetO sequences.

In the present study, we used HT1080 cells (derived from a fibrosarcoma) as they show a stable karyotype near diploid ($2n = 46$), which we thought is best suited for gene-targeting experiments (knock-in experiments). Only a few of human cell lines, like HT1080 and HCT116, etc., are suited for gene targeting, and above all, HT1080 has been utilized for mutation assay in several studies.

However, this cell line turned out to have a spontaneous mutation rate somewhat higher than that in normal cells; namely, it was estimated as 12×10^{-6}/cell division in HT1080 cells (resistance to 6TG) [18] while the rates for normal cells are, for example, $0.45–1.8 \times 10^{-6}$/cell generation in human skin fibroblasts (resistance to 8-azaguanine) [26] or $0.055–0.24 \times 10^{-6}$ [27], or $5–10 \times 10^{-6}$ [28] in human blood lymphocytes (resistance to 6TG), although the published data varies extensively. We felt that the elevated level of spontaneous mutation rate of HT1080 cells could be related to the characteristics of its stable karyotype; namely, chromosomal instability (CIN) and mismatch-repair deficiency leading to microsatellite instability (MIN) are often mutually exclusive (but not necessarily so) in colorectal cancers, and HT1080 cells are at least non-CIN and normal regarding the p53 gene status [29]. However, we did not find any indication that the cells are MIN; namely, the spectrum of base-change mutations at the *TetR* gene did not indicate any clustering at microsatellite or repeat sequences. In any event, to maintain the spontaneous mutation rate low in the control culture, it would probably be beneficial, for example, to use cells of

non-tumor origin and expressing *hTERT* gene so that natural aging processes may be avoided.

It has long been known that radiation-induced mutation rates varied considerably among genes. For example, among the 7 loci examined by Russell et al., *s* gene mutated much more frequently than other genes and the difference was about 20-fold when compared with the frequency at *a* gene, which was the lowest [30]. Since a positive correlation has been seen between the spontaneous and radiation-induced mutation rates in mouse gene loci, it was once imagined that the difference could be partly due to physical gene size; that is, the larger the gene size, the higher both spontaneous and radiation-induced mutation rates would be. However, following genome sequencing studies, gene size turned out not to matter any longer; for example, *s* and *a* genes consist of 7 and 4 exons and span about 29 kb and 37 kb, respectively. Alternatively, since radiation-induced mutations often accompany large deletions, the presence of vital gene(s) near the marker gene may also be a factor to be considered, while only a limited set of information is thus far available (some papers by Russell's group). Other factors, such as different chromatin conformation, can be part of the reason, but there is practically no relevant information available with regard to radiation mutagenesis. To pursue the issue, *TetR* gene can be inserted at any locus in the genome of cultured cells as the reporter of mutations provided that the locus is stably expressed under the normal culture conditions.

Finally, if the present system is realized in an *in vivo* mouse system, it would become possible to obtain three sets of data simultaneously; namely, quantitative data necessary for evaluation of mutagenicity *in vivo*, tissue dependence of the activity, and carcinogenicity, which may help better understanding the role of somatic mutations in carcinogenesis. There are two major hurdles to be cleared, however; one is identifying the effective promoter that may work on different tissues, and the other is choosing the sites for single integrations of each of *TetR* and *TetO/FGP* genes into the genome.

Conflict of interest statement

The authors declare that there are no conflicts of interest.

Acknowledgements

We thank Drs. Charles Waldren and Evan Douple for their kind comments and discussion. The Radiation Effects Research Foundation (RERF), Hiroshima and Nagasaki, Japan, is a private, non-profit foundation funded by the Japanese Ministry of Health, Labour and Welfare (MHLW) and the US Department of Energy (DOE), the latter through the National Academy of Sciences. This publication was supported by RERF Research Protocol RP-1-08, Central Research Institute of Electric Power Industry (CRIEPI), and by a Grant-in-Aid for Scientific Research (s) (21221003) from the Ministry of Education, Sports, Science and Technology (MEXT) of Japan.

Appendix A. Supplementary data

Supplementary data associated with this article can be found, in the online version, at doi:10.1016/j.mrgentox.2010.12.010

References

[1] J. McCann, B.N. Ames, Detection of carcinogens as mutagens in the Salmonella/microsome test: assay of 300 chemicals: discussion, Proc. Natl. Acad. Sci. U.S.A. 73 (1976) 950–954.
[2] V. Thybaud, M. Aardema, J. Clements, K. Dearfield, S. Galloway, M. Hayashi, D. Jacobson-Kram, D. Kirkland, J.T. MacGregor, D. Marzin, W. Ohyama, M. Schuler, H. Suzuki, E. Zeiger, Strategy for genotoxicity testing: hazard identification and risk assessment in relation to in vitro testing, Mutat. Res. 627 (2007) 41–58.
[3] R.J. Albertini, R. Demars, Diploid azaguanine-resistant mutants of cultured human fibroblasts, Science 169 (1970) 482–485.
[4] D. Clive, Recent developments with the L5178Y TK heterozygote mutagen assay system, Environ. Health Perspect. 6 (1973) 119–125.
[5] A.J. Bishop, B. Kosaras, R.L. Sidman, R.H. Schiestl, Benzo(a)pyrene and X-rays induce reversions of the pink-eyed unstable mutation in the retinal pigment epithelium of mice, Mutat. Res. 457 (2000) 31–40.
[6] D.J. Winton, M.A. Blount, B.A. Ponder, A clonal marker induced by mutation in mouse intestinal epithelium, Nature 333 (1988) 463–466.
[7] J.A. Gossen, J. Vijg, *E. coli* C: a convenient host strain for rescue of highly methylated DNA, Nucleic Acids Res. 16 (1988) 9343–9345.
[8] J.A. Gossen, W.J. de Leeuw, C.H. Tan, E.C. Zwarthoff, F. Berends, P.H. Lohman, D.L. Knook, J. Vijg, Efficient rescue of integrated shuttle vectors from transgenic mice: a model for studying mutations in vivo, Proc. Natl. Acad. Sci. U.S.A. 86 (1989) 7971–7975.
[9] L. Huang, S. Grim, L.E. Smith, P.M. Kim, J.A. Nickoloff, O.G. Goloubeva, W.F. Morgan, Ionizing radiation induces delayed hyperrecombination in Mammalian cells, Mol. Cell. Biol. 24 (2004) 5060–5068.
[10] D.M. Wiktor-Brown, C.A. Hendricks, W. Olipitz, B.P. Engelward, Age-dependent accumulation of recombinant cells in the mouse pancreas revealed by in situ fluorescence imaging, Proc. Natl. Acad. Sci. U.S.A. 103 (2006) 11862–11867.
[11] G. Lozano, R.R. Behringer, New mouse models of cancer: single-cell knockouts, Proc. Natl. Acad. Sci. U.S.A. 104 (2007) 4245–4246.
[12] W. Wang, M. Warren, A. Bradley, Induced mitotic recombination of p53 in vivo, Proc. Natl. Acad. Sci. U.S.A. 104 (2007) 4501–4505.
[13] M.D. Muzumdar, L. Luo, H. Zong, Modeling sporadic loss of heterozygosity in mice by using mosaic analysis with double markers (MADM), Proc. Natl. Acad. Sci. U.S.A. 104 (2007) 4495–5000.
[14] J.M. Fischer, J.R. Stringer, Visualizing loss of heterozygosity in living mouse cells and tissues, Mutat. Res. 645 (2008) 1–8.
[15] C. Gasche, C.L. Chang, L. Natarajan, A. Goel, J. Rhees, D.J. Young, C.N. Arnold, C.R. Boland, Identification of frame-shift intermediate mutant cells, Proc. Natl. Acad. Sci. U.S.A. 100 (2003) 1914–1919.
[16] C. Healy, M. Wade, A. McMahon, A. Williams, D.A. Johnson, C. Parfett, Flow cytometric detection of tandem repeat mutations induced by various chemical classes, Mutat. Res. 598 (2006) 85–102.
[17] V.N. Dobrovolsky, L.J. McGarrity, S.M. Morris, R.H. Heflich, Detection of mutation in transgenic CHO cells using green fluorescent protein as a reporter, Mutat. Res. 518 (2002) 55–64.
[18] A. Noda, Y. Kodama, H.M. Cullings, N. Nakamura, Radiation-induced genomic instability in tandem repeat sequences is not predictive of unique sequence instability, Radiat. Res. 167 (2007) 526–534.
[19] R.D. Palmiter, R.R. Behringer, C.J. Quaife, F. Maxwell, I.H. Maxwell, R.L. Brinster, Cell lineage ablation in transgenic mice by cell-specific expression of a toxin gene, Cell 50 (1987) 435–443.
[20] A. Tachibana, K. Tatsumi, T. Masui, T. Kato, Large detetions at HPRT locus associated with the mutator phenotype in a Bloom's Syndrome lymphoblastoid cell line, Mol. Carcinog. 17 (1996) 41–47.
[21] A. Nádas, E.I. Goncharova, T.G. Rossman, Maximum likelihood estimation of spontaneous mutation rates from large initial populations, Mutat. Res. 351 (1996) 9–17.
[22] A. Nadas, E.I. Goncharova, T.G. Rossman, Mutations infinity: improved statistical methods for estimating spontaneous rates, Environ. Mol. Mutagen 28 (1996) 90–99.
[23] P.L. Foster, Sorting out mutation rates, Proc. Natl. Acad. Sci. U.S.A. 96 (1999) 7617–7618.
[24] S. Luria, M. Delbrück, Mutation of bacteria from virus sensitivity to virus resistance, Genetics 28 (1943) 491–511.
[25] M.C. Cimino, Comparative overview of current international strategies and guidelines for genetic toxicology testing for regulatory purposes, Environ. Mol. Mutagen 47 (2006) 362–390.
[26] R. DeMars, Resistance of cultured human fibroblasts and other cells to purine and pyrimidine analogues in relation to mutagenesis detection, Mutat. Res. 24; (1974) 335–364.
[27] R. Seshadri, R.J. Kutlaca, K. Trainor, C. Matthews, A.A. Morley, Mutation rate of normal and malignant human lymphocytes, Cancer Res. 47 (1987) 407–409.
[28] R.J. Albertini, J.A. Nicklas, J.P. O'Neill, Somatic cell gene mutations in humans: biomarkers for genotoxicity, Environ. Health Perspect. 101 (Suppl. 3) (1993) 193–201.
[29] S. Sharma, I. Schwarte-Waldhoff, H. Oberhuber, R. Schäfer, Functional interaction of wild-type and mutant p53 transfected into human tumor cell lines carrying activated ras genes, Cell Growth Differ. 4 (1993) 861–869.
[30] A.G. Searle, Mutation induction in mice, Adv. Radiat. Biol. 4 (1974) 131–207.

The Impact of Superior Mediastinal Lymph Node Metastases on Prognosis in Non-small Cell Lung Cancer Located in the Right Middle Lobe

Yukinori Sakao, MD, PhD, Sakae Okumura, MD,* Mun Mingyon, MD, PhD,* Hirofumi Uehara, MD, PhD,* Yuichi Ishikawa, MD, PhD,† and Ken Nakagawa, MD**

Background: We aimed to assess hilar and mediastinal lymph node involvement and its impact on prognosis in patients with right middle lobe lung cancer.

Methods: The records of 170 patients undergoing surgery for right middle lobe non-small cell lung cancer from 1980 to December 2007 were retrospectively examined. There were 45 patients found to have hilar or mediastinal lymph nodes metastases. This subgroup included 31 N2 patients and 14 N1 patients, and included 23 women and 22 men, whose ages ranged from 32 to 83 years (median = 61 years). The status of mediastinal, hilar, and interlobar lymph nodes was assessed according to the seventh edition of the TNM classification for lung cancer. Patient records were examined for age, gender, preoperative nodal status, surgical procedure, metastatic status of lymph nodes (distribution and numbers), tumor size, and histologic features (cell type and differentiation degree). Survival duration was defined as the interval between surgery and death from the tumor or the most recent follow-up.

Results: For N1 cases (n = 14), the most frequent metastatic site was #12m (lymph nodes adjacent to the middle lobe bronchus), which occurred in 11 cases; there was one case with metastases in #11s (lymph nodes between the upper lobe bronchus and bronchus intermedius), and no case with #11i metastases (lymph nodes between the right middle and lower lobe bronchi). The most frequent metastatic mediastinal zone was the subcarinal zone (25/31), and the superior mediastinal zone also had a high incidence of metastases (22/31). Sixteen cases had metastases to both the superior and subcarinal zones, and six cases had metastasis to superior mediastinal zone without subcarinal zone metastasis. When #11s or #11i was involved, eight of nine or five of five, respectively, were N2 cases. Univariate analyses revealed that tumor diameter, cN, status of lymph node metastases, and operative procedure (pneumonectomy) were significant prognostic factors in N2 cases. Regarding status of lymph node metastases, superior mediastinal zone metastases, both superior and inferior (subcarinal) zone metastases, and #11i were significant prognostic factors. Because #11i metastases and superior mediastinal lymph nodes metastases were highly correlated with each other (p = 0.02), two separate models were used in multivariate analyses. Superior mediastinal metastases (p = 0.03) and #11i metastases (p = 0.015) were revealed to be significant independent prognostic factors, whereas multiple-zone metastases only tended toward significance as an adverse prognostic factor (p = 0.054).

Conclusions: Superior mediastinal lymph node metastases and #11i metastases were significant adverse prognostic factors in patients with middle lobe lung cancer, and they were associated with each other.

Key Words: Middle lobe cancer, Superior mediastinal lymph node metastasis, N2, NSCLC.

(*J Thorac Oncol.* 2011;6: 494–499)

The right middle lobe is the smallest lobe in the lung, and lung cancer originating there is much less common than in the other lobes, occurring in 3.8 to 6.7% of all lung cancers.[1–4] The fact that it is less common may be a reason that there are a few reports on the prognostic factors of middle lobe lung cancer.

Lymph drainage from the middle lobe extends to both superior and inferior mediastinal lymph nodes, and previous reports have demonstrated a high incidence of metastases to both the superior and inferior mediastinal zones.[1–6] Nevertheless, there are few articles on the relationships between status of hilar and mediastinal lymph node metastases and patient prognoses.

In this retrospective study, we aimed to clarify prognostic factors in patients with middle lobe lung cancer who underwent surgery. Furthermore, we wanted to determine the association between the status of lymph node metastases and postoperative prognosis.

PATIENTS AND METHODS

This was a retrospective study. Because individual patients were not identified, our institutional review board waived the requirement for obtaining patient consent and approved this study. Between 1980 and December 2007, 170 patients underwent surgical resection at the Cancer Institute

Departments of *Thoracic Surgical Oncology and †Pathology, Japanese Foundation for Cancer Research, Cancer Institute Hospital, Tokyo, Japan.

Disclosure: The authors declare no conflicts of interest.

Address for correspondence: Yukinori Sakao, MD, PhD, Department of Thoracic Surgical Oncology, Japanese Foundation for Cancer Research, Cancer Institute Hospital, 3-10-6, Ariake, Koto-ku, Tokyo 135-8550, Japan. E-mail: yukinori.sakao@jfcr.or.jp

ISSN: 1556-0864/11/0603-0494

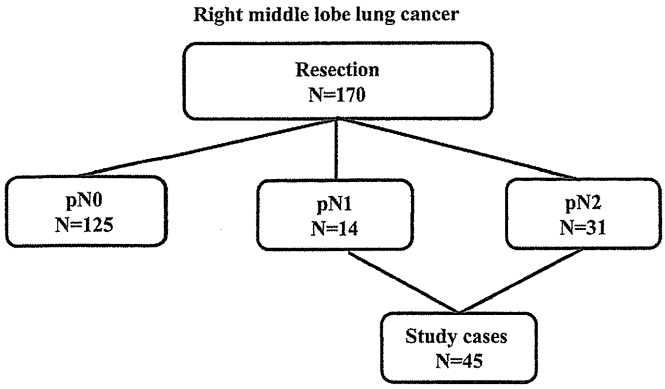

FIGURE 1. Study group subdivisions. Between 1980 and December 2007, 170 patients underwent surgical resections for right middle lobe lung cancer at the Cancer Institute Hospital. There were 14 N1 cases and 31 N2 cases evaluated.

Hospital for primary lung cancer originating in the right middle lobe. Among these patients, 45 were diagnosed with N1 or N2 disease after lung resection and hilar and mediastinal node dissections (Figure 1). The extent of lymph node dissection was not affected by a suspicion of N1 disease. We have routinely performed nearly the same dissection (ND2a).

All the 45 study patients were confirmed for their prognoses. The primary surgical procedure for lymph node dissection, such as hilar and mediastinal nodal dissection, was established in Japan in the late 1970s. In our institute, the extent of lymph node dissection conducted recently is nearly the same as that during the 1980s. Some cases had sampling due to disorders such as cardiac or pulmonary, and these cases were excluded from this study. The resected lymph nodes were separated according to the map[7] in the operating room by the surgeons. Station 10 nodes dissected in middle lobe cancer were adjacent to the inferior parts of the main bronchus, and these nodes were included in the subcarinal zone according to the new TNM. [7] The other station 10 nodes, which were adjacent to the upper parts of the main bronchus, were not routinely dissected, and this area is difficult to dissect without an upper lobectomy.

This subgroup included 31 N2 patients and 14 N1 patients, and included 23 women and 22 men, whose ages ranged from 32 to 83 years (median = 61 years, Table 1). For all patients, preoperative staging was performed using chest computed tomography (CT), abdominal CT or ultrasonography, brain CT or magnetic resonance imaging, and bone scans. Clinical mediastinal and hilar lymph node status was assessed as positive if the chest CT showed that the short axis of a node was more than 1.0 cm. CT scans have been used for evaluating lung cancer staging in our institute since 1980. Of course, CT imaging quality is different when comparing that in the 1980s with that in the 2000s. Nevertheless, this study focused on pathological N status of middle lobe lung cancer, and the quality of pathological examinations was nearly the same during the study period. We excluded those patients who had induction therapy because it seemed to be difficult to evaluate their pathological node status.

TABLE 1. Patient Characteristics

Age (yr)	32–83, median: 61
Gender (male/female)	22/23
c-N	
N0/N1/N2	23/14/8
c-T	
T1/T2/T3/T4	17/24/3/1
p-N	
N1/N2	14/31
Histologic type	
Adenocarcinoma/others	35/10
Well-differentiated/others	10/35
Surgical procedure	
Lobectomy/bilobectomy/pneumonectomy	21/14/10

Bulky N2 (shortest mediastinal lymph node diameter >2 cm) patients have not been candidates for surgery in our institute. Although mediastinoscopy, 18F-fluorodeoxyglucose positron emission tomography, or endobronchial ultrasound with transbronchial needle aspiration was applied to some patients in this series, they were not used for preoperative staging. Follow-up periods ranged from 2 to 302 months (median follow-up for living patients was 86 months).

The status of mediastinal, hilar, or interlobar nodes was assessed according to the seventh edition of the TNM classification for lung cancer.[7] Mediastinal nodes were classified into the following three zones: superior, subcarinal, and inferior. N1 nodes were classified into two zones as hilar or interlobar, and peripheral. The interlobar zone was divided into three subgroups as follows: #12m, lymph nodes adjacent to the middle lobe bronchus; #11s, lymph nodes between the upper lobe bronchus and bronchus intermedius; and #11i, lymph nodes between the right middle and lower lobe bronchi. When a case had mediastinal nodal involvement of two or more zones, it was classified with multiple-zone metastases.

Patient characteristics are summarized in Table 1. Patient records were examined for age, gender, preoperative nodal status, surgical procedure, metastatic status of lymph nodes (distribution and numbers), tumor size, and histologic features (cell type and degree of differentiation).

Statistical Analysis

Survival duration was defined as the interval between surgery and death from the tumor, or the most recent follow-up. Survival rates were calculated using the Kaplan-Meier method. Univariate analyses were performed using the log-rank test, χ^2 test, and logistic regression. Multivariate analyses were performed for variables with p values less than 0.1 by univariate analysis, using the logistic regression test in StatView J 5.0 (SAS Institute Inc., Cary, NC). A p value less than 0.05 was considered significant.

RESULTS

Status of Lymph Node Metastases

In N1 cases (n = 14), the most frequent metastatic site was #12m, occurring in 11 cases, and there was one case with metastases in #11s and 0 cases with #11i metastases (Figure 2).

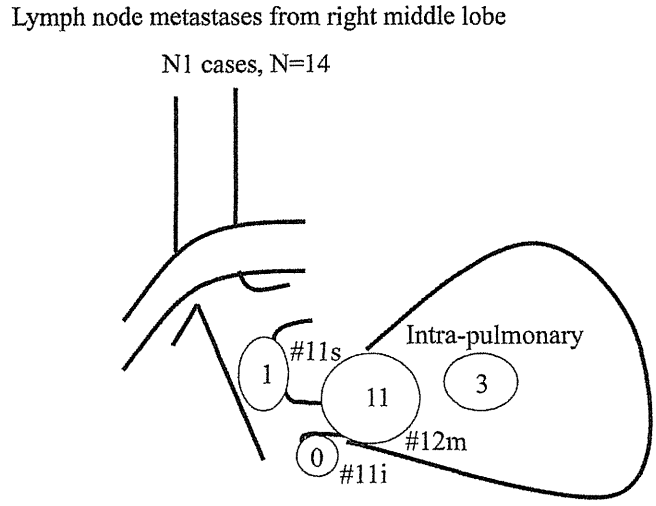

FIGURE 2. Distribution of metastatic nodes in N1 cases.

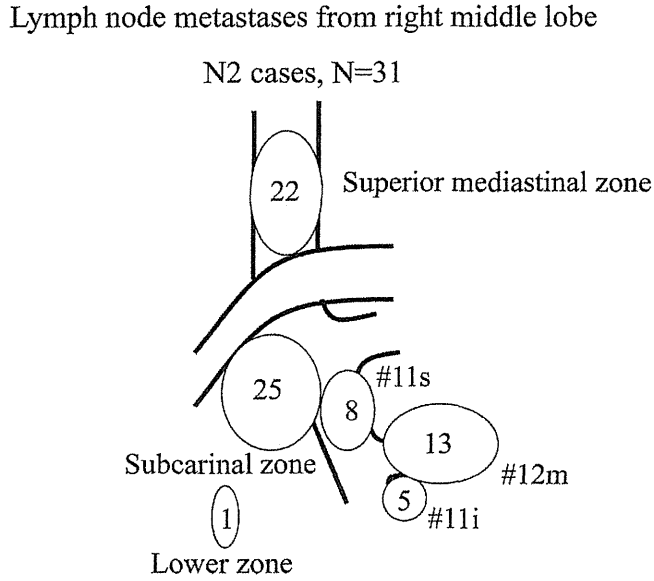

FIGURE 3. Distribution of metastatic nodes in N2 cases.

The most frequent metastatic mediastinal zone was the subcarinal zone (25/31 N2 cases). The superior zone also had a high incidence of metastases (22/31 cases). There were 16 cases with metastases in both the superior and subcarinal zones; nine cases were metastasized to the subcarinal zone without the superior mediastinal zone metastasis, and six cases were metastasized to superior the mediastinal zone without the subcarinal zone metastasis (Figure 3). When #11s was involved, eight of nine cases were N2, and when #11i was involved, all five cases were N2 (Figures 4 and 5).

Survival Rates for Patients with Nodal Involvement

The postoperative 5-year survival rate for patients with N1 was 62% and with N2 was 20% ($p = 0.02$). The postoperative 5-year survival rate was 83% for 125 N0 patients. The prognoses for N0 patients with right middle lobe cancers were not different from those of N0 patients with other involved lobes.

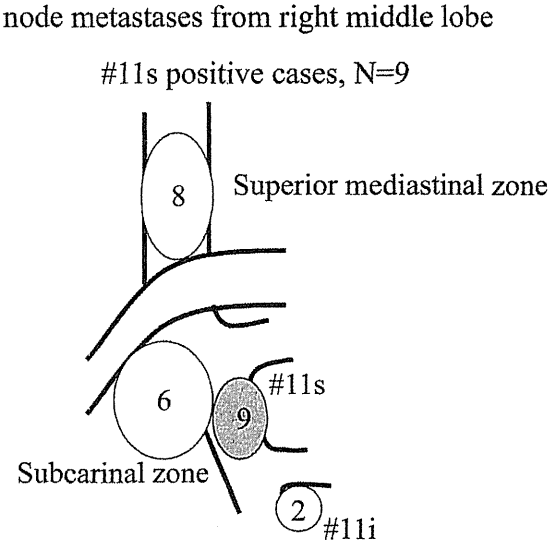

FIGURE 4. Association of #11s metastases with mediastinal zone metastases.

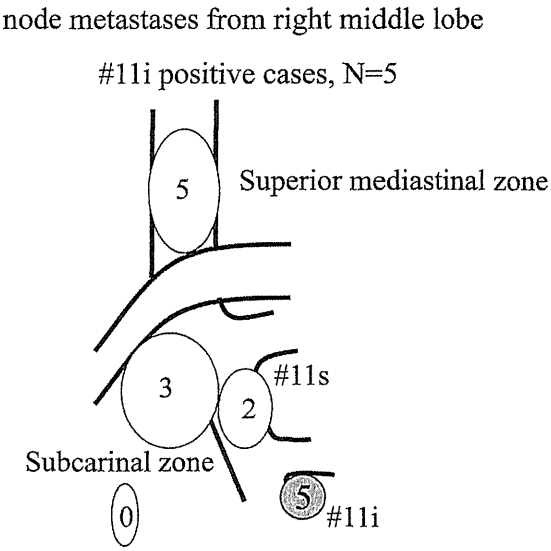

FIGURE 5. Association of #11i metastases with mediastinal zone metastases.

Prognostic Factors for N2 in the Right Middle Lobe

Univariate analyses using the variables listed in Table 2 showed that diameter, cN1–2/cN0, status of lymph node metastases, and operative procedure (pneumonectomy) were significant prognostic factors. Nevertheless, there was no difference in prognoses between lobectomy and bilobectomy. Regarding specific prognostic lymph node metastases, superior mediastinal zone metastases, both superior and subcarinal and interlobar #11i metastases were significant prognostic factors. Inferior mediastinal zone metastases, and #12m and

TABLE 2. Prognostic Factors for Patients with N2: Univariate Analysis

Variables	Cases	5-yr Survival (%)	*p*
Gender			
Male/female	14/17	17.8/22.0	0.95
Age			
<70 yr/70 yr or older	22/9	21.7/16.0	0.37
Diameter (14–65 mm, mean: 35 mm)			
<35 mm/35 mm or larger	16/15	36.5/6.8	0.02
cN			
cN1–2/cN0	15/16	8.0/33.7	0.042
cN0–1/cN2	23/8	23.3/12.5	0.24
Adenocarcinoma/others	26/5	25.2/0	0.1
Well differentiated/others	6/25	16.7/21.5	0.81
Pleural involvement yes/no	15/16	21.8/17.3	0.57
Status of lymph node metastases			
Superior mediastinal zone yes/no	22/9	6.4/50.8	0.005
Inferior mediastinal zone yes/no	25/6	21.4/16.7	0.61
#12m yes/no	13/18	24.7/18.3	0.92
#11s yes/no	8/23	14.3/21.9	0.14
#11i yes/no	5/26	0/23.6	0.02
Both superior and inferior zones			
Multiple zones/single zone	16/15	0/36.4	0.01
Operative procedure			
Pneumonectomy vs. others	7/24	0/25.8	0.009
Lobectomy vs. bilobectomy	16/8	23.6/29.2	0.61
Period			
Before 1995 vs. from and after 1995	15/16	13.3/28.4	0.28

#12m, lymph nodes adjacent to middle lobe bronchus; #11s, lymph nodes between the upper lobe bronchus and bronchus intermedius; #11i, lymph nodes between the right middle and lower lobe bronchi.

TABLE 3. Prognostic Factors for Patients with N2: Multivariate Analysis

Variables	Odds Ratio	95% CI	*p*
Model 1			
Diameter	1.04	0.99–1.08	0.054
cN			
cN1–2/cN0	1.87	0.71–4.95	0.21
Status of lymph node metastases			
Superior mediastinal zone	5.08	1.20–21.8	0.03
Multiple zones	1.42	0.51–3.96	0.50
Operative procedure			
Pneumonectomy	1.13	0.30–4.34	0.88
Model 2			
Diameter	1.03	0.99–1.06	0.17
cN			
cN1–2/cN0	1.38	0.54–3.52	0.51
Status of lymph node metastases			
#11i	4.80	1.34–17.0	0.015
Multiple zones	2.80	0.98–7.96	0.054
Operative procedure			
Pneumonectomy	2.32	0.62–10.0	0.20

#11i, lymph nodes between the right middle and lower lobe bronchi.

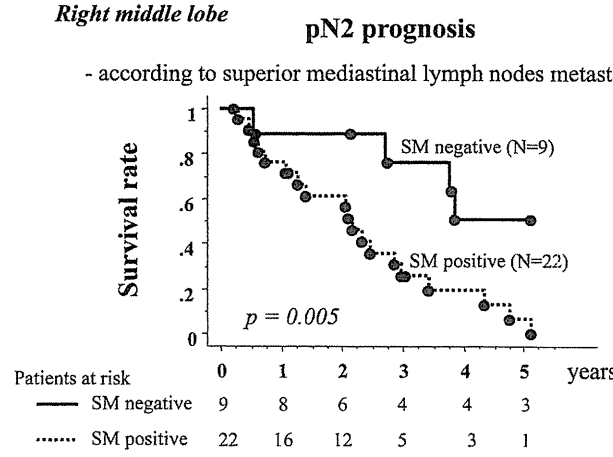

FIGURE 6. Postoperative survival according to superior mediastinal nodal involvement.

#11s metastases were not significant. There was no difference in prognoses between the patients before 1995 and patients from 1996 and after (5-year survivals of 13.3% and 28.4%; $p = 0.28$).

Significant variables by univariate analyses were analyzed by multivariate analyses (Table 3, models 1 and 2). Because #11i metastases and superior mediastinal lymph nodes metastases were highly correlated with each other ($p = 0.02$), two separate models were used for multivariate analyses. In model 1, superior mediastinal metastases were revealed to be a significant independent prognostic factor ($p = 0.03$). In model 2, #11i metastases were revealed to be a significant independent prognostic factor ($p = 0.015$), whereas multiple zone metastases only tended toward significance as an adverse prognostic factor ($p = 0.054$).

Survival Rate According to Prognostic N2 Factors

N2 patients were categorized according to whether they had significant prognostic factors determined from multivariate analyses, including superior mediastinal lymph nodes metastases, #11i metastases, or multiple mediastinal metastatic zones.

The 5-year survival rate was 50.8% in patients without superior mediastinal lymph nodes metastases, whereas it was 6.4% in patients with superior mediastinal lymph node metastases ($p = 0.005$, Figure 6). The 5-year survival rate was 23.6% in patients without #11i lymph node metastases, whereas there were no long-term survivors (dead within 3 years) in patients with #11i lymph node metastases ($p = 0.008$, Figure 7). Furthermore, the 3-year and 5-year survival rates were 58.2% and 36.4% in patients with single-zone mediastinal lymph node metastases, whereas they were 29.6% and 0% in patients with multiple-zone mediastinal lymph node metastases ($p = 0.01$), respectively. Nevertheless, by multivariate analysis, superior mediastinal lymph

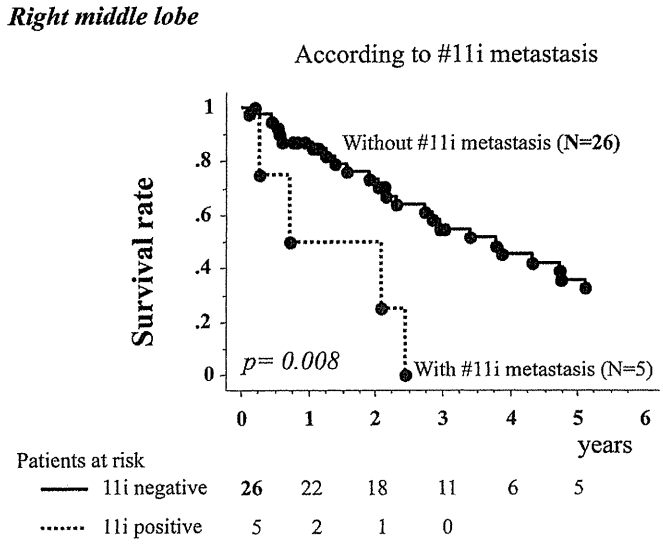

FIGURE 7. Postoperative survival according to #11i nodal involvement.

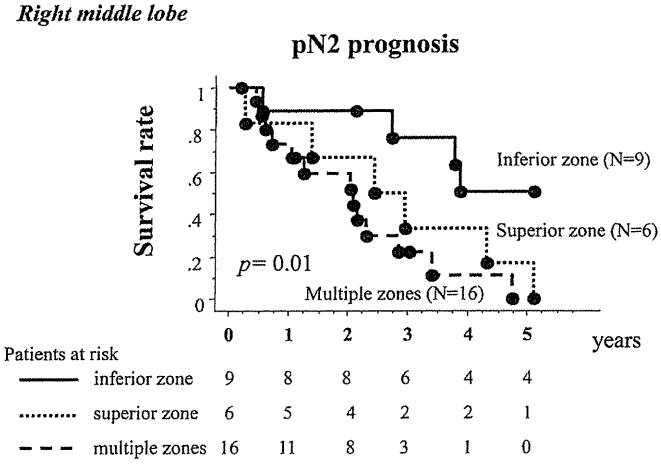

FIGURE 8. Postoperative survival: comparison of superior mediastinal nodal involvement with multiple-zone metastases.

node metastases were revealed to be a stronger prognostic factor than multiple metastatic zones (Figure 8).

DISCUSSION

There have been many reports on the prognostic impact of metastasis to specific mediastinal zones, especially lung cancer in the upper or lower lobes. For patients with lung cancer with tumor originating in the upper lobe or division, the frequency of subcarinal lymph node metastases has been reported to range from 3 to 5%, with the 5-year survival rates ranging from 9 to 18%.[8–10] The frequency of superior mediastinal lymph node metastases has been reported to range from 4 to 5%, with 5-year survival rates ranging from 0 to 19%.[10,11] This low-frequency mediastinal lymph node involvement was highly associated with multilevel N2, and therefore, the outcomes were poor.[10,12,13] In this study, the frequency of metastases was similar for the subcarinal and superior mediastinal zones, and the incidences in N2 patients were 80.6% and 71.0%, respectively. Thus, both superior and inferior mediastinal zones were found to be major metastatic sites, and these results are compatible with previous reports.[14]

We have revealed that metastases to the superior mediastinal lymph nodes are an important independent prognostic factor in patients with N2 middle lobe cancer. This is similar to what is seen in lower lobe cancer. Nevertheless, the incidence of skip metastasis to the superior mediastinum is very different between cancer in the middle lobe and in the lower lobe. The incidence in this study was 20% for N2 and has been reported to range from 3 to 4.5% in N2 right lower lobe cancer.[10–12] Furthermore, there was a significant difference in the 5-year survival rates for superior mediastinal involvement and inferior mediastinal involvement (6.5% and 50.8%, respectively), even for single-zone N2. When superior mediastinal lymph nodes were involved, the prognosis was almost the same as for multilevel N2 patients with middle lobe cancer.

The most frequent metastatic hilar lymph node was #12m, and most #11s and #11i metastases were found in N2 patients. In other words, metastases found in #11s or #11i indicate N2 disease (#11s: 8/9 and #11i: 5/5). Surprisingly, interlobar (lower lobe: #11i) lymph node involvement was an important adverse prognostic factor, even in N2 patients. This may be explained by the fact that there was an association between #11i metastases and superior mediastinal nodal involvement. Metastasis in #11i may be understood to be a result of mediastinal nodal involvement. That is, #11i metastasis is retrograde because of disturbed antegrade lymph drainage to the superior mediastinum from mediastinal metastases. Unfortunately, we could not find any previous reports regarding this correlation between #11i and superior mediastinal node involvement. Further investigation is needed to prove the hypothesis that #11i metastases result from superior mediastinal lymph node metastases.

In conclusion, superior mediastinal lymph node metastases and #11i metastases were significant adverse prognostic factors in patients with middle lobe lung cancer, and they were associated with each other. Furthermore, in patients with middle lobe lung cancer, #11i metastases may result from mediastinal metastases, and the impact on prognosis must be different from that of patients with cancer in other lobes.

Limitations of this study include its retrospective nature, including cases from the 1980s, a small sample number, and that routine adjuvant chemotherapy for N2 patients was started in 2006. Therefore, in this study, it was difficult to evaluate the effects on prognosis with respect to adjuvant chemotherapy.

REFERENCES

1. Vincent RG, Takita H, Lane WW, et al. Surgical therapy of lung cancer. *J Thorac Cardiovasc Surg* 1976;71:581–591.
2. Freise G, Gabler A, Liebig S. Bronchial carcinoma and long-term survival. Retrospective study of 433 patients who underwent resection. *Thorax* 1978;33:228–234.

3. Gifford JH, Waddington JKB. Review of 464 cases of carcinoma of lung treated by resection. *Br Med* 1957;30:723–730.
4. Ochsner A, Ray CJ, Acreea PW. Cancer of lung; review of experiences with 1457 cases of bronchogenic carcinoma. *Am Rev Tuberc* 1954;70:763–783.
5. Riquet M, Dupont P, Hidden G, et al. Lymphatic drainage of the middle lobe of the adult lung. *Surg Radio Anat* 1990;12:231–233.
6. Hata E, Hayakawa K, Miyamoto H, et al. Rationale for extended lymphadenectomy for lung cancer. *Thorac Surg* 1990;5:19–25.
7. Rusch VW, Asamura H, Watanabe H, et al. Members of IASLC Staging Committee. The IASLC lung cancer staging project: a proposal for a new international lymph node map in the forthcoming seventh edition of the TNM classification for lung cancer. *J Thorac Oncol* 2009;4:1043–1045.
8. Asamura H, Nakayama H, Kondo H, et al. Lobe-specific extent of systematic lymph node dissection for non-small cell lung carcinomas according to a retrospective study of metastasis and prognosis. *J Thorac Cardiovasc Surg* 1999;117:1102–1111.
9. Uehara H, Okumura S, Satoh Y, et al. Validity of omission of subcarinal lymph node dissection in patients with cancer of the right upper lobe or left upper division of the lung. *Jpn J Lung Cancer* 2008;48:266–272.
10. Okada M, Sakamoto T, Yuki T, et al. Border between N1 and N2 stations in lung carcinoma: lessons from lymph node metastatic patterns of lower lobe tumors. *J Thorac Cardiovasc Surg* 2008;129:825–830.
11. Uehara H, Sakao Y, Mun M, et al. Prognostic value and significance of subcarinal and superior mediastinal lymph node metastasis in lower lobe tumours. *Eur J Cardiothorac Surg* 2010;38:498–502.
12. Ichinose Y, Kato H, Koike T, et al. Japanese Clinical Oncology Group. Completely resected stage IIIA non-small cell lung cancer: the significance of primary tumor location and N2 station. *J Thorac Cardiovasc Surg* 2001;122:803–808.
13. Sakao Y, Miyamoto H, Yamazaki A, et al. The prognostic significance of metastasis to the highest mediastinal lymph node in non-small cell lung cancer. *Ann Thorac Surg* 2006;81:292–297.
14. Naruke T, Tsuchiya R, Kondo H, et al. Lymph node sampling in lung cancer: how should it be done? *Eur J Cardiothorac Surg* 1999;16:S17–S24.

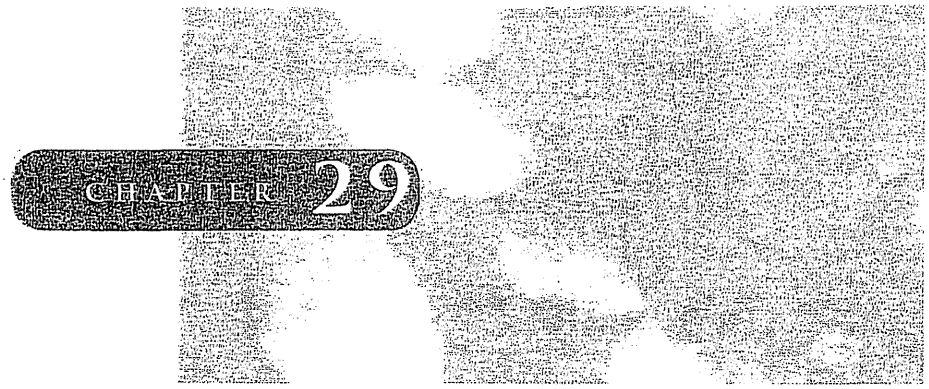

Molecular Diagnostics of Esophageal and Gastric Cancers

Wataru Yasui, Naohide Oue, Kazuhiro Sentani, and Dongfeng Tan

INTRODUCTION

Gastric cancer is the fourth most common cancer worldwide, and mortality from gastric cancer is second only to that of lung cancer.[1] The areas with the highest rates of gastric cancer are in Eastern Asia, South America, and Eastern Europe. Of note, approximately 60% of all gastric cancers occur in Japan, China, and Korea. The incidence of gastric cancer is declining worldwide, mainly due to changes in eating habits such as decreased consumption of high-salt diets and availability of fresh fruits and vegetables throughout the year. One of the most important etiologic factors is *Helicobacter pylori* (HP) infection. Infection with HP causes chronic atrophic gastritis and intestinal metaplasia, conditions that are considered as predisposing to cancer development. In Japan and to some degree in Korea, screening for early disease by double-contrast barium X-ray followed by endoscopy has been widely performed. Advances in endoscopic diagnosis and treatment have enabled us to offer excellent long-term survival for patients with early cancer. However, in other parts of the world, the majority of gastric cancers are diagnosed as advanced disease after symptoms appear, and prognosis of advanced cancer remains poor.

Esophageal cancer is the sixth most common human malignant disease worldwide, with more than 400,000 new cases per year.[2] Two major types, squamous cell carcinoma (SCC) and adenocarcinoma, account for over 95% of esophageal cancers. SCC commonly occurs in developing countries and is typically associated with consumption of tobacco and alcohol. Adenocarcinoma typically occurs in white men in developed countries, and the important etiologic factors are obesity, chronic gastro-esophageal reflux, and Barrett esophagus. Although endoscopic screening is useful for early cancer detection, 50% of superficial esophageal cancers (those confined to the submucosa) have nodal metastasis. Most esophageal cancers are diagnosed at an advanced stage, and prognosis after surgical resection with neoadjuvant chemoradiotherapy remains unsatisfactory; the 5-year survival rate is <50% after curative surgery.

Cancer is a chronic proliferative disease that develops and progresses by accumulation of multiple genetic and epigenetic alterations. Great efforts have been made to clarify the precise molecular mechanisms of esophageal and gastric carcinogeneses. Multiple alterations include abnormalities in tumor suppressor genes, oncogenes, growth factors and receptors, DNA mismatch repair genes, cell adhesion molecules, and matrix metalloproteinases.[3-6] In recent years, the role of microRNA (miRNA) in epigenetic regulation and biologic function in cancers has been extensively studied.[7] Better knowledge of molecular carcinogenesis will lead to new methods of diagnosis and treatment. At present, although molecular-targeted therapy has been introduced widely against a variety of cancers, for esophago-gastric and gastric cancers only trastuzumab against HER2 has been approved for clinical use in advanced cases. Molecular diagnosis still remains challenging in the practical setting. This chapter describes molecular diagnosis of gastric and esophageal cancers and possible clinical implications (Table 29.1).

TABLE 29-1 Molecular Diagnosis of Esophageal and Gastric Cancers and Its Clinical Implication

Diagnosis	Method	Implication
DNA methylation–targeted diagnosis	Methylation-specific PCR and bisulfite sequencing	Detection, aggressiveness, prognosis, and serum marker
Molecular target	IHC and FISH/DISH	Target detection and patient selection
Micrometastasis	RT-PCR and OSNA	Detection of cancer cells and CTC
miRNA-based diagnosis	RT-PCR and microarray	Detection, aggressiveness, prognosis, and serum marker
Genetic polymorphism	Sequencing and RFLP	Cancer risk, efficacy, and toxicity of chemotherapy

IHC, immunohistochemistry; FISH, fluorescence in situ hybridization; DISH, dual-color silver-enhanced in situ hybridization; CTC, circulating tumor cell; OSNA, one-step nucleic acid amplification; RFLP, restriction fragment length polymorphism; PCR, polymerase chain reaction; RT-PCR, reverse transcription–polymerase chain reaction.

MOLECULAR DIAGNOSIS OF GASTRIC CANCER

Molecular Pathologic Diagnosis Routinely Implemented

From 1993 to 2000, a project was implemented to perform molecular diagnosis using histopathologic samples from the gastrointestinal tract as a routine service.[3,9] This system of molecular diagnosis was designed mainly for the differential diagnosis of benign and malignant tumors, diagnosis of the degree of malignancy, and identification of susceptibility to multiple primary cancers (Fig. 29.1). Molecular examination was performed on about 5,000 gastric lesions, and much useful information in addition to histopathologic findings was obtained. During routine microscopic observation, pathologists observed cancer, adenoma/dysplasia, borderline lesions, and suspicious lesions of neoplasia. The sections were immunostained for molecular markers (including p53, TGF-α, EGF, EGFR, c-met, c-erbB2/HER2, cyclin E, p27, and CD44) for differential diagnosis and/or evaluation of degree of malignancy. With polymerase chain reaction (PCR)–single-strand conformation polymorphism and PCR–restriction fragment length polymorphism, deletion and mutation of *APC* and *p53* genes were examined by the pathologist using portions of formalin-fixed, paraffin-embedded, hematoxylin and eosin–stained sections. For detection of genetic instability, human mutL homolog 1 (hMLH1) staining was used for screening, and genetic instability was assessed by microsatellite assay using four loci of CA repeats and two poly(A) tracts. Ten percent of histologically diagnosed adenomas were diagnosed as adenoma with malignant potential and 2% were considered suspicious for adenocarcinoma. Adenocarcinoma was identified in more than 20% of histologically diagnosed borderline lesions. Twelve percent of adenocarcinomas were regarded as showing high-grade malignancy, and their prognosis

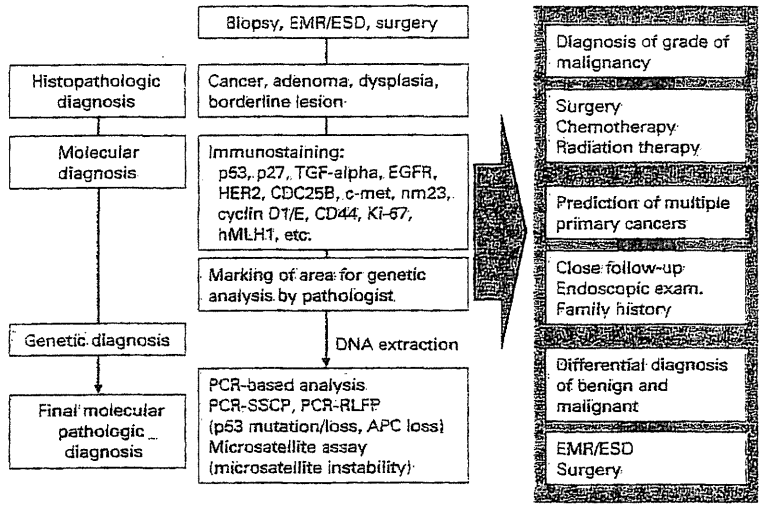

FIGURE 29–1 Proposed workflow of molecular evaluation of esophageal and gastric cancers. EMR (endoscopic mucosal resection), ESD (endoscopic submucosal dissection), PCR (polymerase chain reaction), SSCP (single strand conformation polymorphism), RFLP (restriction fragment length polymorphism), APC (adenomatous polyposis coli)